

Transition-Metal Tailored Ga₂O₂ Monolayer: From Room-Temperature Gas Sensing to Chemical Scavenging

Afreen Anamul Haque¹ and Aniket Singha¹

¹Department of E & ECE, IIT Kharagpur, India

*Email:afreenhaque28@gmail.com

Abstract

Pristine Ga₂O₂ monolayers suffer from poor sensitivity and weak molecular capture, limiting their application in toxic gas detection and environmental detoxification. Here, we employ first-principles density functional theory (DFT) calculations to investigate the gas sensing and scavenging properties of Ga₂O₂ monolayers substitutionally tailored via seven transition-metals (TM): Pd, Zn, Zr, Mo, Ag, Ti, and Pt. All TM-substituted monolayers exhibit negative formation and binding energies, negligible lattice distortion, and structural stability in molecular dynamics simulations. Performance evaluation against eight toxic industrial and three environmental gases reveals functionalities ranging from selective, reusable room-temperature sensing to permanent molecular capture. Ag substitution exhibits exceptional selectivity for NO with moderate adsorption strength ($\sim -0.83\text{eV}$), an up to eight-order-of-magnitude conductivity enhancement, besides facilitating reusable O₂ and NO₂ detection. Additionally, Pd, Zn, Zr, and Mo substitutions tune selectivity toward NO, NO₂, CO₂, CO, and O₂. Coming to applications towards toxic gas capture, Zr- and Mo-substituted systems selectively scavenge oxidizing gases, whereas Ti and Pt act as universal scavengers. Further analysis reveals that, Pd- and Ag-substituted monolayers remain selective for NO, while Zn substitution favors NO₂ detection even in ambient atmospheric conditions. Thus, these tailored Ga₂O₂ monolayers offer a practical platform for atmospheric monitoring and detoxification.

Keywords

2D materials based gas sensors, Density Functional Theory (DFT), Novel Ga₂O₂-based gas sensors, substitution, molecule scavenging

1 Introduction

The detection and capture of hazardous gas molecules at trace concentrations is a challenge of growing urgency across environmental monitoring, industrial safety, and biomedical diagnostics. Toxic species such as NO, NO₂, SO₂, NH₃, H₂S, CO, CS₂ etc. are implicated in urban air pollution, respiratory disease, and industrial process hazards and pose critical risks in confined environments [1, 2]. Additionally, HF, a highly corrosive compound widely encountered in semiconductor fabrication and chemical processing industries, poses severe toxicity hazards even at trace concentrations. Hence, the detection of these molecules has become quite imperative.

Recently, two-dimensional (2D) materials have emerged as compelling candidates for next-generation gas sensing platforms owing to their high surface-to-volume ratio, tunable electronic properties, and compatibility with miniaturized device architectures [3–8]. A wide range of 2D materials including graphene [3, 9], transition metal dichalcogenides [10], hexagonal boron nitride [11–13], and metal oxide monolayers [14–17] etc., are being explored for sensing applications. The particular class of 2D-metal oxides have attracted growing attention due to their intrinsic semiconducting character and rich surface chemistry, which enable

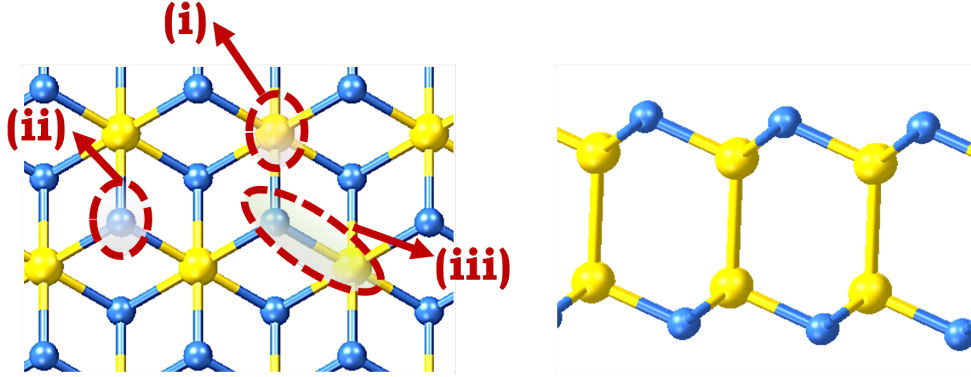


Figure 1: Left Panel: Top view of the 2D Ga_2O_2 monolayer along with the schematic representation of the three sites considered for transition-metal substitution: (i) Ga-site substitution, where the TM replaces a Ga atom; (ii) O-site substitution, where the TM replaces an O atom; and (iii) Stone–Wales (SW) defect-site substitution, where the TM occupies the site created by the Stone–Wales defect. The location of the substitution sites have been encircled in red color. Right Panel: Side view of the pristine Ga_2O_2 monolayer.

diverse molecule–surface interactions [14]. Unlike conventional bulk metal oxide gas sensors, which often require elevated operating temperatures because of their wide bandgaps, 2D metal oxides offer the possibility of lower temperature operation due to their reduced bandgaps, compared to their bulk counterparts [18, 19]. All these advantages further make them promising candidates for room-temperature gas sensing applications. Among the emerging members of this family, a recently proposed two-dimensional phase of Gallium Oxide with stoichiometric formula Ga_2O_2 has attracted growing interest owing to its structural stability, oxidation resistance, moderate electronic bandgap of 2.76eV (HSE06) and high hole mobility [20–25]. The Ga_2O_2 monolayer (ML) adopts a buckled, graphene-like structure stabilized by strong directional Ga–O bonding (see Fig. S1 in Supporting Information (SI)). This moderate bandgap may facilitate adsorption-induced conductivity modulation at room temperature, making the Ga_2O_2 ML a promising candidate to study for gas sensing applications. In a prior investigation, we established the intrinsic gas sensing characteristics of the pristine Ga_2O_2 ML, demonstrating selective detection of NH_3 at room temperature as its primary sensing capability, with NO detection accessible only under low-temperature conditions [26]. However, the adsorption energy for most other hazardous gas species remain modest in the pristine ML. This hampers the possibility of detecting molecules other than NH_3 and also precludes irreversible molecular capture limiting the material’s broader sensing and scavenging potential.

Substitutional doping with transition metal (TM) atoms offers a direct and chemically versatile route to overcome these limitations [27–30]. By introducing dopant-specific d-states in the bandgap, TM substituents fundamentally reshape the electronic landscape of the host ML, enabling interactions with target analytes beyond those facilitated by the pristine surface [31]. Transition metals spanning the periodic table differ systematically in their d-band occupation, electronegativity, and atomic radius, each introducing a distinct local electronic and structural perturbation to the Ga_2O_2 lattice. Early transition metals such as Ti (Z=22) [11, 12] and Zr (Z=40) [32, 33], together with middle- and late-series dopants including Zn (Z=30) [34, 35], Mo (Z=42) [36], Pd (Z=46) [37–39], Ag (Z=47) [40, 41], and Pt (Z=78) [38, 42, 43], possess chemically accessible d states that facilitate strong adsorbate–surface hybridization and charge redistribution, thereby profoundly influencing molecular adsorption characteristics. This systematic progression across the transition metal series provides a rational basis for exploring a wide functional landscape, from selective room-temperature sensing to irreversible molecular scavenging. In this work, a comprehensive adsorption and sensing investigation of the TM substituted Ga_2O_2 ML is carried out across eleven gas species, comprising eight hazardous analytes: NH_3 , NO, SO_2 , NO_2 , H_2S , CO, CS_2 . To gauge the possibility of deploying in ambient environment, the interaction of the substituted ML with three ambient atmospheric gases such as O_2 , CO_2 , and H_2O are also explored. Owing to the chemically inert nature of N_2 , its interaction with the surface is not examined in detail.

This paper is organized as follows. In Sec. 2, we highlight the details of our computational methodology and the specifics of the parameters employed for calculations. Next, in Sec. 3, we discuss the gas sensing performance of the substituted Ga₂O₂ ML, where we first discuss the adsorption properties (Sec. 3.1) and then proceed towards discussing its performance as a reusable gas sensor and as a scavenger. We conclude the paper briefly in Sec. 4.

2 Computational Methods

First-principles density functional theory (DFT) calculations were performed using the Vienna *ab initio* Simulation Package (VASP). The exchange-correlation interactions were treated within the generalized gradient approximation (GGA) using the Perdew-Burke-Ernzerhof (PBE) functional in the projector augmented wave (PAW) framework [44–46]. For Ga, the semicore d-states were treated as valence states to properly assess bonding with the neighbouring atoms and adsorption of gas molecules. The substituted metal atoms were described using the corresponding PAW pseudo-potentials, with semicore p states included in the valence configuration where available. A $4 \times 4 \times 1$ supercell was constructed to study the adsorption characteristics of the gas molecules. Structural optimization of the supercell was carried out using a $3 \times 3 \times 1$ Monkhorst-Pack k-point mesh and a plane-wave cutoff energy of 500eV . Gaussian smearing with a width of 0.05eV was employed to facilitate electronic convergence during structural relaxation and self-consistent field (SCF) calculations. For the density of states (DOS) calculations, the tetrahedron method was used for Brillouin-zone integration to obtain accurate electronic occupations and DOS features. A vacuum layer of approximately 25\AA was introduced along the out-of-plane direction to avoid spurious interlayer interactions arising from periodic boundary conditions. The van der Waals interactions were incorporated using Grimme’s DFT-D3 method with zero damping [47, 48]. All calculations were considered converged when the total energy difference between successive self-consistent field iterations was below 10^{-8}eV and the maximum residual force on each atom was less than $10^{-4}\text{eV}/\text{\AA}$.

Table 1: Calculated values of formation energy (E_f) and binding energy (E_{bind}) of the most energetically favorable configuration for all the seven substituted monolayers under consideration.

Element	Formation Energy E_f , (eV)	Binding Energy E_{bind} , (eV)	Environmental Conditions
Ti	-3.92	-4.83	O-rich
Zn	-5.05	-9.31	O-rich
Zr	-6.86	-17.63	O-rich
Mo	-2.27	-16.64	O-rich
Pd	-2.31	-9.16	O-rich
Ag	-3.29	-9.11	O-rich
Pt	-1.16	-5.35	O-rich

The converged in-plane lattice constant of the pristine supercell was found to be 12.47 \AA . To determine the preferred substitution site for a TM atom, we modeled three cases in the Ga₂O₂ monolayer: (i) TM substituting a Gallium atom (Ga vacancy), (ii) TM substituting an Oxygen atom (O vacancy), and (iii) TM incorporated at a Stone–Wales (SW) defect, as demonstrated in Fig. 1. Each dopant atom (Ti, Zn, Zr, Mo, Pd, Ag, and Pt) was substituted at these defect sites followed by full structural relaxation (see Fig. S2 in SI). Out of the three cases, the configuration with the lowest formation energy is most likely to form spontaneously. Hence, this configuration was selected for further investigation of gas sensing capabilities. The values of the formation energy for the most probable configuration in each case is given in Table 1. In addition to the formation energy, the thermodynamic stability of the most stable configuration of each of the seven substituted systems was evaluated using the calculated binding energy and molecular dynamics (MD) simulations. For gas adsorption studies, the gas molecules were initially positioned at a vertical distance of 2.5\AA above the ML surface at the site of TM substitution. For each gas molecule, three initial adsorption geometries, namely; one parallel configuration and two perpendicular configurations to the plane of ML were

examined. In the perpendicular arrangements, each terminal atom of polar molecules was separately oriented toward the substituted TM site to account for orientation-dependent adsorption effects due to dipole formation. The relaxed configurations for all the adsorption cases under investigation has been included in SI.

3 Results and Discussion

As stated in the last section, the relative formation probabilities of all the substituted configurations under investigation were evaluated through the calculation of the corresponding formation energies (E_f). Formation energy is defined as the energy required to form a defect or substitutional configuration in a material relative to the pristine structure. A negative formation energy indicates that the defect or substitution is likely to form spontaneously. For a defect configuration, E_f is calculated as:

$$E_f = E_{tot}^{sub} - \mu_{sub} + m\mu_{Ga} + n\mu_O - E_{tot}^{PL}, \quad (1)$$

where E_{tot}^{sub} is the total energy of the TM atom-substituted Ga_2O_2 ML, E_{tot}^{PL} is the total energy of the pristine ML and μ_{sub} corresponds to the average chemical potential of the substitutional atom in the most stable bulk phase. Here, m and n represent the number of Ga and O atoms removed, respectively. The chemical potentials of μ_{Ga} and μ_O under Ga-rich and O-rich conditions, respectively, were obtained from the average energies of the corresponding most stable reference phases of these elements under room temperature and normal atmospheric pressure. On the other hand, the values for μ_{Ga} and μ_O for O-rich and Ga-rich conditions, respectively, were calculated using the following expression [49–51] :

$$4\mu_{Ga} = 2\mu_{Ga_2O_3} - 3\mu_{O_2}, \quad (2a)$$

$$3\mu_O = \mu_{Ga_2O_3} - 2\mu_{Ga}, \quad (2b)$$

In the above equation, $\mu_{Ga_2O_3}$ represents the average chemical potential of β - Ga_2O_3 , which is the most stable oxide of Gallium [52–54]. Among the considered configurations, TM substitution at the Ga site under O-rich conditions was found to exhibit the lowest formation energy and thus, is considered as energetically favourable. In all the cases, the energetically favourable substitution configuration demonstrated negative formation energy (Table 1) hinting towards the possibility of spontaneous formation under O-rich conditions. In addition, the binding energy (E_{bind}) was calculated using the expression:

$$E_{bind} = E_{tot}^{sub} - E_{tot}^{vac} - \mu_{sub}, \quad (3)$$

where E_{tot}^{vac} is the total energy of the ML containing the corresponding vacancy. All the TM substitutions under consideration display negative binding energies, indicating attractive interaction between the TM atom and the host lattice, thereby suggesting structural stability. In addition, the average change in the in-plane lattice constant in each of these cases was noted to be less than 1%, highlighting negligible structural distortion on substitution with the TM atoms. To evaluate the finite-temperature thermodynamic stability of the substituted Ga_2O_2 monolayer, Ab-initio Molecular Dynamics (AIMD) simulations were carried out for all seven dopant configurations at 1000 K. In all cases, the energy fluctuations remain bounded without noticeable systematic drift, and no structural degradation or dopant migration is observed in any of the simulation, indicating good dynamical stability of the substituted systems. The corresponding AIMD plots depicting temporal energy fluctuation at $T = 1000K$ are included in the Fig. S3 in SI.

3.1 Adsorption Characteristics

To gauge the possibility of reasonable interaction of the gas molecules with TM-substituted ML, the adsorption energy (E_{ads}) was calculated by using the expression given below:

$$E_{ads} = E_{tot}^{sub + molecule} - E_{tot}^{molecule} - E_{tot}^{sub}, \quad (4)$$

where $E_{tot}^{sub + molecule}$ is the total energy of the substituted system alongwith the molecule and $E_{tot}^{molecule}$ is the total energy of the isolated molecule. To classify stable adsorption at and around room temperature, a lower

bound of -0.4eV was imposed on the adsorption energy [14, 55–57]. Adsorption energies weaker than (less negative) -0.4eV implies that thermal fluctuations under ambient conditions may result in rapid desorption with recovery times too short for reliable electrical detection. In this work, adsorption energies in the range of -0.4eV to -1eV are considered optimal for reusable gas sensing, as they provide a balance between stable adsorption and spontaneous surface regeneration under ambient conditions. Adsorption energies between -1eV and -1.5eV remain potentially useful for gas sensing; however, surface regeneration may necessitate thermal annealing or UV-assisted desorption. When adsorption energies surpass -1.5eV , the interaction is effectively irreversible under practical operating conditions, rendering the material more suitable as a one time sensor or molecular gas scavenger rather than a reusable detection platform. Accordingly, the adsorption energy window of -0.4eV to -1.5eV is adopted here as the favorable regime for gas capture, with the sub-ranges distinguished according to their expected recovery characteristics as explained earlier. In addition to adsorption energy, the adsorption height (H) and net charge transfer (Q) between the adsorbate and adsorbent also provide valuable insights into the nature of adsorption. Adsorption height refers to the perpendicular distance between the parent layer and the molecule in the most stable configuration. To achieve stable and robust adsorption, a reasonable level of charge transfer between the substrate and the molecules is essential. Bader Partition Algorithm [58] was employed to compute the charge distribution and assess the charge transfer between the substituted Ga_2O_2 ML and the gas molecule and was calculated using the expression Eq. S1 in SI. In order to assess the reusability of the gas sensors, we have also computed the recovery time (τ) using Arrhenius equation, Eq. S2 given in SI. We note that the recovery time should be of the order of milliseconds to few seconds for both suitable electrical detection and spontaneous surface regeneration in a reusable gas sensor.

While these descriptors provide a comprehensive picture of the strength, stability, and reversibility of adsorption, they do not directly reveal whether adsorption can induce a measurable electrical response. Since the operating principle of a resistive gas sensor relies on adsorption-induced modifications to the electronic structure of the sensing layer, a detailed analysis of the electronic density of states (DOS) is required to establish the sensing capability of the material toward a given analyte. Therefore, in addition to adsorption attributes, we systematically examine the modification of the electronic DOS upon exposure to each target gas molecule. Adsorption of target molecules might induce electronic perturbations such as gap state formation, Fermi level shifts, and changes in the effective bandgap of the adsorbate-ML system which often reflects as a change in the conductance of the system. These features reveal the donor or acceptor character of each adsorbate and its effect on the mobile carrier population. Together, they provide a rigorous electronic basis for interpreting the expected changes in electrical conductivity upon adsorption. Throughout this paper, electron excitation energy refers to the minimum energy required for an electron to transition from a completely or partially filled state to the conduction band edge (CBE). Analogously, hole excitation energy refers to the minimum energy required to excite a hole in the valence band (VB) and is given by the energy difference between the valence band edge (VBE) and the closest completely or partially unoccupied state.

In what follows, we present a systematic analysis of the interaction between gas molecules and TM-substituted Ga_2O_2 ML for each of the seven TM species. We evaluate the adsorption characteristics, electronic structure modifications, and conductometric response for all of the analytes under consideration. Based on the adsorption energy, recovery time, charge transfer and modulation in DOS, each substitution case is assessed for its suitability as a reusable resistive gas sensor, or a molecular scavenger or none, establishing a comprehensive dopant-dependent functional classification of the substituted Ga_2O_2 ML.

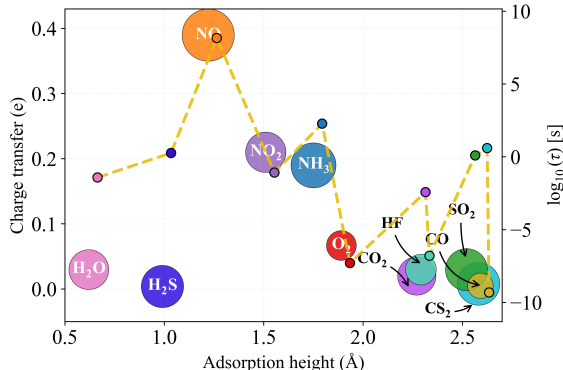
3.2 Pd Substitution

Pd substitution produces a broad spectrum of adsorption responses across the investigated analytes. The corresponding values of E_{ads} , Q, H, and τ for all the considered gas molecules on Pd-substituted ML (Pd- Ga_2O_2) are summarized in Fig. 2. Molecules such as O_2 ($E_{ads}=-0.28\text{eV}$), CO (-0.16eV) and HF (-0.31eV) display adsorption energies above (greater than) the -0.4eV threshold, characteristic of weak adsorption behaviour and insufficient for stable signal detection. Accordingly, their DOS hasn't been investigated in detail. A different adsorption regime was observed for molecules like NH_3 (-0.85eV), SO_2 (-0.72eV), NO_2 (-0.65eV),

H₂S ($-0.73eV$), CO₂ ($-0.57eV$), H₂O ($-0.63eV$), and CS₂ ($-0.75eV$). They exhibited adsorption energies within the favorable range for reusable sensing.

Molecule	E_{ads} (eV)	H (Å)	q (e)	τ (s)
NH ₃	-0.83	1.75	0.19	1.90×10^2
NO	-1.20	1.22	0.39	1.44×10^8
SO ₂	-0.72	2.52	0.03	1.25
O ₂	-0.28	1.89	0.067	5.06×10^{-8}
NO ₂	-0.65	1.51	0.21	8.31×10^{-2}
H ₂ S	-0.73	0.99	0.004	1.83
H ₂ O	-0.63	0.62	0.03	3.83×10^{-2}
CO	-0.16	2.59	0.005	4.87×10^{-10}
CO ₂	-0.57	2.27	0.02	3.76×10^{-3}
CS ₂	-0.75	2.58	0.008	3.98
HF	-0.31	2.29	0.03	1.61×10^{-7}

(a)



(b)

Figure 2: (a) Table I: Adsorption parameters of the investigated gas molecules on the Pd-Ga₂O₂ ML, including adsorption energy (E_{ads}), adsorption height (H), charge transfer (q), and recovery time (τ). (b) Graphical summary of the adsorption characteristics of gas molecules on the Pd-Ga₂O₂ monolayer. The centers of the larger bubbles are referenced to the X and primary Y-axes, representing the adsorption height and charge transfer, respectively. The area of each bubble is proportional to the magnitude of the adsorption energy. The smaller markers linked by the dashed line indicate the corresponding recovery times, referenced to the secondary Y-axis. Recovery times are reported on a logarithmic scale.

DOS analysis of the Pd-Ga₂O₂ ML reveals a localised partially filled state at the Fermi level, with contributions dominated by the Pd atom and its immediate coordination environment (see Fig. 3). This state, located approximately $0.35eV$ above the VBE, imparts an elevated baseline p-type conductivity or the doping effect, against which adsorption-induced conductivity modulations must be assessed. It is noteworthy that oxides of Gallium are commonly reported to exhibit intrinsic n-type behavior due to inherent donor impurities introduced during synthesis or fabrication processes [53, 59–63]. In contrast, Pd substitution induces a p-type behaviour in the Ga₂O₂ ML, whereas the remaining TM substituents examined in this work preserve the n-type behavior.

NH₃ adsorption does not significantly alter the position of the adsorption-induced states relative to the Pd-Ga₂O₂ ML. The partially filled state remains at the Fermi level, located approximately $0.35eV$ above the VBE, closely resembling the Pd-Ga₂O₂ ML (see Fig. S6 in SI). As a result, the dominant excitation pathway remains between the VBE and this partially filled state, thereby retaining the predominantly hole-mediated (p-type) conductivity of the system. Consequently, the hole excitation energy remains essentially unchanged, suggesting that the conductivity of the system will remain largely unaffected by NH₃ adsorption. Accordingly, NH₃ is not identified as a target analyte for Pd-Ga₂O₂ ML.

In contrast, for H₂S, H₂O, CS₂, and SO₂ adsorption, the dominant excitation occurs in CB. In the case of H₂S and H₂O, the electron excitation energy ($0.32eV$ and $0.37eV$, respectively) to CBE is comparable to the hole excitation energy to the VBE in the Pd-substituted ML. As a result, the net carrier excitation energy remains largely unchanged. Under these circumstances, the lower electron mobility becomes the dominant distinguishing factor, suggesting a reduction in conductivity upon the adsorption of these species. Nevertheless, owing to the comparable excitation energies associated with the electron mediated transport channel in the analyte adsorbed Pd-Ga₂O₂ ML and hole mediated transport channels in the Pd-Ga₂O₂ ML without the analyte, the magnitude of the resulting conductivity modulation cannot be inferred reliably from the present analysis since the two transport channels are associated with different carrier mobility. However we do not expect a reliable significant change in the conductivity and the change may be modulated by other factors including unintentional impurity or defects in the ML.

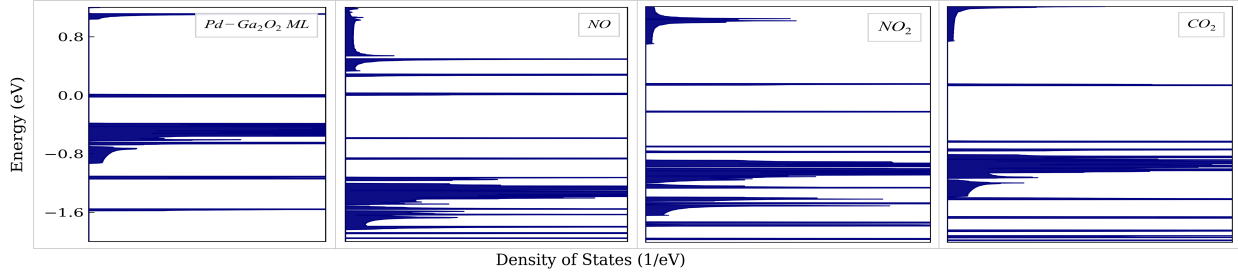


Figure 3: Total DOS of the Pd-Ga₂O₂ ML and upon adsorption of the favorable target molecules. The Fermi level is pinned at 0eV in all the panels.

In the case of CS₂ and SO₂ adsorption, we note electron excitation energy of 0.27eV and 0.28eV respectively, which are smaller than the corresponding hole excitation energy. This might result in enhanced carrier excitations in the former case. However, it is also noteworthy that the electron mobility (μ_e) in Ga₂O₂ is an order of magnitude less compared to the hole mobility (μ_h) [20], which compensates the possibility of conductivity enhancement due to stronger electron excitation in the molecule adsorbed ML to some extent. These competing factors make it difficult to reliably predict either the magnitude or the polarity of the resulting conductivity modulation from the present analysis alone. Accordingly, the precise conductivity response of the all the four aforementioned molecules such as H₂S, H₂O, CS₂, and SO₂ adsorbed systems remains beyond the scope of the present theoretical study and is left for future experimental investigation. However, we do not expect sufficient conductometric response from adsorption of these molecules and hence these are not considered as target molecules for detection by Pd-Ga₂O₂ ML.

In the case of CO₂ adsorption, the dominant excitation occurs in the CB. In this case, the electron excitation energy of 0.53eV is larger than the hole excitation energy of the Pd-Ga₂O₂ ML (see Fig. 3). This is expected to suppress the conductivity. Furthermore, since the dominant transport channel is electron-mediated in the adsorbed ML and the electron mobility (μ_e) is substantially lower than the hole mobility (μ_h), this effect is anticipated to further reinforce the conductivity suppression. Consequently, CO₂ may serve as a viable target analyte for reusable sensing on the Pd-Ga₂O₂ ML. Although CO₂ is an ambient species, such a response could be particularly useful in controlled or enclosed environments where accurate monitoring of CO₂ concentration is of practical interest.

NO₂ adsorption also substantially alters the electronic structure of the Pd-Ga₂O₂ ML. In this case, we note a hole excitation energy (to the VB) of 0.95eV and electron excitation energy (to the CB) of 0.84eV. Consequently, the excitation of electrons and holes are associated with significantly larger energy requirement compared to that of Pd-Ga₂O₂ ML, leading to a suppression of the electrical conductivity.

It is noted that, unlike the aforementioned molecules, NO exhibits an adsorption energy of $-1.20eV$, placing it in the borderline adsorption regime where reusable sensing remains feasible, although complete surface recovery may require thermal annealing or UV-assisted desorption. DOS analysis reveals that NO adsorption eliminates the partially filled Fermi-level state present in the Pd-Ga₂O₂ ML. Consequently, the relevant excitations are governed by the gap between VBE and the lowest unoccupied state, located approximately at 1.2eV above it or on the CB and the highest occupied state located at 0.88eV below it. This substantial increase in the effective excitation energy relative to the Pd-Ga₂O₂ ML is expected to significantly suppress the electrical conductivity. Thus, NO, NO₂ and CO₂ are identified as suitable target analytes for reusable sensing on the Pd-Ga₂O₂ ML, exhibiting both favorable adsorption characteristics and adsorption-induced conductivity suppression.

Selectivity Analysis of NO and NO₂ sensing under ambient conditions: To understand the selectivity of the Pd-Ga₂O₂ ML in the ambient environment, we need to understand the detectability of these

gases in the presence of CO_2 . As discussed above, in addition to NO and NO_2 ; CO_2 also exhibits stable adsorption on $\text{Pd-Ga}_2\text{O}_2$ and is predicted to induce a measurable conductometric response. Since CO_2 is present at reasonable concentrations, it is important to evaluate whether competition for active sites from CO_2 , hampers the detectivity of NO and NO_2 in the ambient environment. To this end, adsorption site occupancy probabilities were computed using the grand canonical adsorption model (Section 3.1, Eq. S3, SI) [64] considering NO and NO_2 at 25 ppm (regulatory permissible exposure limit [65, 66]) in the presence of O_2 (21%), alongside N_2 (79%), H_2O (5000 ppm), and CO_2 (400 ppm) at 1 atm total pressure. Detailed active site occupancy probability calculations are provided in Section 2.1 of the SI.

For NO , the exceptionally strong adsorption energy (-1.20eV) overwhelmingly outweighs the concentration advantage of the ambient gases, yielding a site occupancy probability approaching unity (see Table S1, SI). Consequently, NO emerges as the dominant surface species under ambient conditions, with negligible competition from O_2 , H_2O , N_2 or CO_2 . This observation further reinforces the suitability of $\text{Pd-Ga}_2\text{O}_2$ for practical NO detection.

In contrast, the occupancy probability of NO_2 is found to be only $\sim 0.26\%$ with CO_2 having comparable probability of $\sim -0.20\%$ as well, under identical conditions (see Table S2, SI). The active sites are predominantly occupied by H_2O ($\sim 97.98\%$), while there is negligible probability for O_2 and N_2 occupancy. Therefore, despite its favorable adsorption energy and predicted conductometric response, practical NO_2 detection is expected to be significantly hindered under ambient conditions due to competition from humidity, and to a lesser extent CO_2 . These results suggest that NO_2 sensing using $\text{Pd-Ga}_2\text{O}_2$ would be more feasible in humidity and CO_2 -controlled environments. Thus, NO emerges as a promising target analyte under ambient conditions; however, its relatively strong adsorption suggests that reusable operation would likely require assisted recovery mechanisms.

3.3 Zn, Zr and Mo Substitution

Zn-substituted System: Among the substituted configurations examined, the Zn-substituted ML ($\text{Zn-Ga}_2\text{O}_2$) presents a particularly nuanced functional picture. The adsorption energies for molecules such as CO_2 ($E_{ads}=-0.25\text{eV}$), CS_2 (-0.35eV), and HF (-0.34eV) fall weaker than -0.4eV threshold, showing unstable adsorption, with recovery times in the sub-microsecond range, precluding any stable signal detection. Since these molecules exhibit weak adsorption characteristics, a detailed DOS analysis was not performed for them.

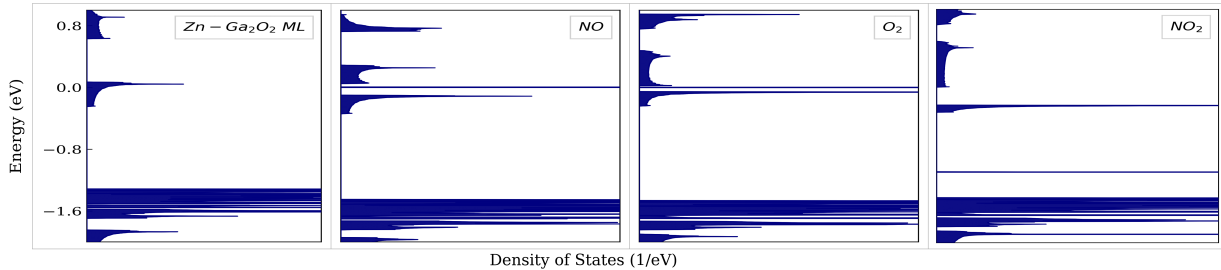


Figure 4: Total DOS of the $\text{Zn-Ga}_2\text{O}_2$ ML and upon adsorption of the favorable target molecules. The Fermi level is pinned at 0eV in all the panels.

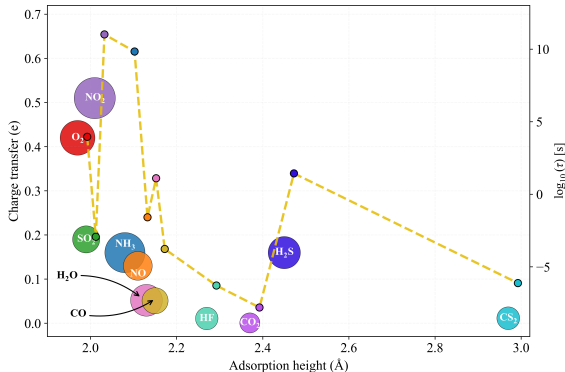
Molecules such as NO (-0.62eV), SO_2 (-0.54eV), CO (-0.49eV), H_2S (-0.80eV), H_2O (-0.78eV), and O_2 (-0.95eV) exhibit adsorption energies within the range between -0.4eV to -1.0eV for reusable gas sensors. DOS analysis of the $\text{Zn-Ga}_2\text{O}_2$ ML (see Fig. 4) reveals a delocalised mini-band like characteristics at the Fermi level, endowing the surface with intrinsic metallic character [67–70]. For adsorbed SO_2 , CO , H_2O , and H_2S , the Fermi level remains within this mini-band-like state (see Fig. S9 in SI), indicating that the

conductivity of the adsorbed systems remains comparable to that of the Zn-substituted monolayer. Therefore, these molecules are not considered as the target analytes for Zn-Ga₂O₂ ML. However, upon adsorption of NO and O₂, the Fermi energy moves outside this delocalised miniband into the forbidden gap, giving rise to an electron excitation energy of 0.15eV ($\approx 6k_B T$) and 0.075eV ($\approx 3k_B T$), respectively at $T = 300K$ (see Fig. 4). This indicates a metal-to-semiconductor transition accompanied by a significant reduction in electrical conductivity.

In contrast to the above case, NH₃ (-1.30eV) and NO₂ (-1.37eV) exhibit strong chemisorptive interactions approaching the -1.5eV irreversibility threshold. Their low adsorption heights and substantial charge transfer (see Fig. 5) further point towards deep chemisorptive adsorption, while the predicted recovery times (see Fig. 5) suggest that surface recovery may only be achievable through external thermal annealing or UV-assisted desorption techniques. Despite the strong adsorption of NH₃, it does not significantly alter the electronic structure of the Zn-Ga₂O₂ ML (see Fig. S9 in SI). The Fermi level continues to penetrate the miniband as present in the Zn-substituted ML, thereby preserving its metallic character. Consequently, NH₃ is not considered a target analyte for the Zn-Ga₂O₂ ML. On the contrary, the adsorption of NO₂ opens a considerably larger energy gap of about 0.235eV ($\approx 10k_B T$ at $T = 300K$), indicating substantial conductivity suppression and a transition from metallic to semiconducting behavior. Nevertheless, as the adsorption energy of NO₂ remains below the -1.5 eV irreversibility criterion, Zn-Ga₂O₂ may still be considered a potential reusable resistive sensing platform for NO₂, provided that externally assisted recovery techniques are employed.

Molecule	E_{ads} (eV)	H (Å)	q (e)	τ (s)
NH ₃	-1.30	2.08	-0.16	6.90×10^9
NO	-0.62	2.11	0.13	2.60×10^{-2}
SO ₂	-0.54	1.99	0.19	1.18×10^{-3}
O ₂	-0.95	1.97	0.42	9.11×10^3
NO ₂	-1.37	2.01	0.51	1.04×10^{11}
H ₂ S	-0.80	2.45	-0.16	2.75×10^1
H ₂ O	-0.78	2.13	-0.05	1.27×10^1
CO	-0.49	2.15	-0.05	1.70×10^{-4}
CO ₂	-0.25	2.37	-0.0008	1.58×10^{-8}
CS ₂	-0.35	2.97	-0.01	7.58×10^{-7}
HF	-0.34	2.27	-0.01	5.15×10^{-7}

(a)



(b)

Figure 5: (a) Table II: Adsorption parameters of the investigated gas molecules on the Zn-Ga₂O₂ ML, including adsorption energy (E_{ads}), adsorption height (H), charge transfer (q), and recovery time (τ). (b) Graphical summary of the adsorption characteristics of gas molecules on the Zn-Ga₂O₂ monolayer. The centers of the larger bubbles are referenced to the X and primary Y-axes, representing the adsorption height and charge transfer, respectively. The area of each bubble is proportional to the magnitude of the adsorption energy. The smaller markers linked by the dashed line indicate the corresponding recovery times, referenced to the secondary Y-axis. Recovery times are reported on a logarithmic scale.

Selectivity Analysis of NO and NO₂ sensing under ambient conditions: It is worth noting that O₂ is an ambient species, but also emerges as a favorable target analyte on Zn-Ga₂O₂, exhibiting both a suitable adsorption energy (-0.95eV) and a pronounced conductometric response. To assess the practical viability of NO and NO₂ detection under ambient conditions, adsorption site occupancy probabilities were evaluated using the same method utilised for Pd-Ga₂O₂. The detailed calculations are provided in the Section 4.1 in SI.

For NO, the calculated occupancy probability is quite negligible ($\sim 10^{-5}$), while O₂ occupies nearly all available active sites $\sim 99.99\%$. This indicates that competitive adsorption from atmospheric O₂ would severely hinder practical NO detection under ambient conditions. In contrast, NO₂ exhibits an occupancy probability of $\sim 99.87\%$, substantially exceeding that of O₂ $\sim 0.13\%$. Therefore, despite its much lower con-

centration, NO_2 effectively outcompetes atmospheric oxygen owing to its significantly stronger adsorption. Consequently, while NO sensing is expected to require O_2 -controlled environments, NO_2 detection should remain viable under ambient conditions, albeit with the requirement of externally assisted recovery owing to its strong chemisorptive interaction.

Zr-substituted System: In the Zr-substituted ML ($\text{Zr-Ga}_2\text{O}_2$), molecules such as SO_2 ($E_{ads}=-0.37\text{eV}$) and CO_2 (-0.09eV) show weak adsorption energies with $E_{ads} > -0.4\text{eV}$. The DOS were not analysed in these cases. On the other hand, a subset of analytes like H_2S (-0.81eV), H_2O (-0.82eV), CO (-0.52eV), CS_2 (-0.51eV), and HF (-0.53eV) exhibit adsorption energies within the -0.4eV to -1.0eV window, satisfying the energy criterion for stable and reversible adsorption. The values of the adsorption energies for all the molecules under consideration have been summarized in Fig. 6. DOS analysis of the $\text{Zr-Ga}_2\text{O}_2$ ML reveals that the Fermi energy penetrates the conduction band, conferring intrinsic metallic character (see Fig. 7a). For these five molecules with E_{ads} in the range of -0.4eV to -1eV , the Fermi energy of the $\text{Zr-Ga}_2\text{O}_2$ ML continues to penetrate the CB upon adsorption, demonstrating metallic behaviour like that of the $\text{Zr-Ga}_2\text{O}_2$ ML. Hence, the conductometric change factor may not be strong enough for robust and reliable detection. In the absence of a strong conductometric signal change, these molecules, despite their favorable adsorption energetics are rendered electrically invisible. Consequently, they cannot be classified as suitable targets for reusable resistive gas sensing on this platform.

Molecule	E_{ads} (eV)	H (Å)	q (e)	τ (s)
NH_3	-1.39	2.42	-0.097	2.24×10^{11}
NO	-1.42	2.06	0.435	7.16×10^{11}
SO_2	-0.37	2.71	0.404	1.64×10^{-6}
O_2	-2.29	1.92	0.6858	2.95×10^{26}
NO_2	-2.86	1.96	0.6274	1.11×10^{36}
H_2S	-0.81	2.90	-0.0757	4.05×10^1
H_2O	-0.82	2.47	-0.0265	5.96×10^1
CO	-0.52	2.60	0.0149	5.44×10^{-4}
CO_2	-0.09	3.45	0.0265	3.25×10^{-11}
CS_2	-0.51	2.79	0.0054	3.70×10^{-4}
HF	-0.53	2.46	-0.004	8.01×10^{-4}

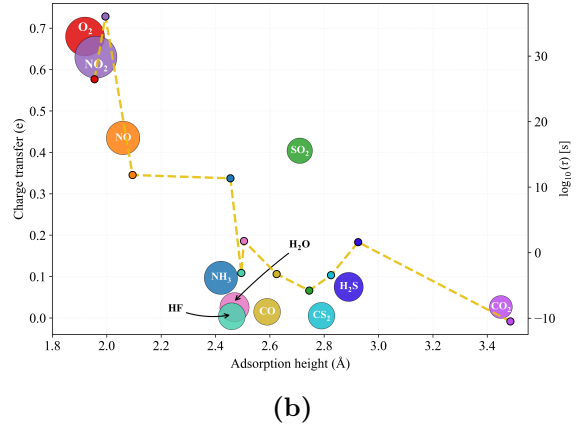


Figure 6: (a) Table III: Adsorption parameters of the investigated gas molecules on the $\text{Zr-Ga}_2\text{O}_2$ ML, including adsorption energy (E_{ads}), adsorption height (H), charge transfer (q), and recovery time (τ). (b) Graphical summary of the adsorption characteristics of gas molecules on the $\text{Zr-Ga}_2\text{O}_2$ monolayer. The centers of the larger bubbles are referenced to the X and primary Y-axes, representing the adsorption height and charge transfer, respectively. The area of each bubble is proportional to the magnitude of the adsorption energy. The smaller markers linked by the dashed line indicate the corresponding recovery times, referenced to the secondary Y-axis. Recovery times are reported on a logarithmic scale.

In contrast, NH_3 (-1.39eV) and NO (-1.42eV) exhibit strong chemisorptive adsorption behaviour approaching but not exceeding the -1.5eV irreversibility threshold. Surface recovery, while impractical under ambient conditions, may in principle be achieved through external thermal annealing or UV photo-desorption treatment. The system remains metallic on adsorption of NH_3 , indicating that the conductivity will not change by an appreciable factor. Consequently, NH_3 is unsuitable as a target analyte for resistive gas sensing. On the other hand, the adsorption of NO shifts the Fermi level out of the CB, thereby inducing an electron excitation energy of 0.85eV ($\approx 33k_B T$ at $T = 300\text{K}$) to the CB (see Fig. 7a). This indicates a transition from metallic to semiconducting behavior, leading to a substantial reduction in conductivity. Therefore, NO can be identified as a promising target analyte for reusable resistive gas sensing with assisted recovery but in O_2 restricted environment (see below).

O_2 (-2.29eV) and NO_2 (-2.86eV) far exceed the -1.5eV threshold for molecular scavenging, exhibiting markedly reduced adsorption heights, substantial charge transfer, and recovery times extending from years

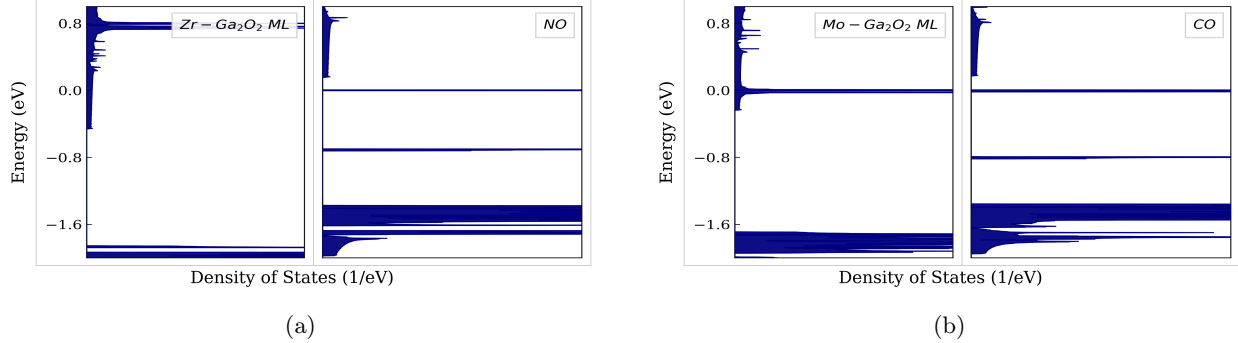


Figure 7: Total DOS of the TM-Ga₂O₂ ML and upon adsorption of the favorable gas molecules: (a) Zr-Ga₂O₂ ML and its target analyte. (b): Mo-Ga₂O₂ ML and its target analyte. The Fermi level is pinned at 0eV in all the panels.

to decades. For both molecules, adsorption drives the Fermi level out of the CB, transforming the metallic Zr-Ga₂O₂ ML into a semiconducting system (see Fig. S12 in SI). In the case of O₂, an excitation energy of approximately 0.49eV is established from the partially occupied state to the CBE, while NO₂ induces a larger excitation energy of 0.68eV. These adsorption-induced electronic modifications are expected to strongly suppress the conductivity of the system. However, owing to the exceptionally strong adsorption strength of O₂ and NO₂, the interaction is more representative of irreversible capture than reusable sensing application. Collectively, these characteristics indicate that the Zr-Ga₂O₂ ML exhibits potential for reusable resistive sensing of NO under controlled operating conditions where competitive adsorption from strongly adsorbed ambient species like O₂ is minimized. Conversely, the strong interactions with O₂ and NO₂ highlight the potential applicability of the Zr-Ga₂O₂ ML for molecular scavenging of these gaseous species.

Mo-substituted System: In the Mo-substituted ML (Mo-Ga₂O₂), the adsorption of SO₂ (1.36eV) is highly unstable in nature as its E_{ads} is positive. Similarly, molecules such as CS₂ ($E_{ads} = -0.32eV$), HF (-0.19eV), and CO₂ (-0.07eV) show weak adsorption behaviour with $E_{ads} > -0.4eV$. In these cases, the DOS has not been analysed in detail. On the other hand, H₂S (-0.61eV), H₂O (-0.61eV), and NH₃ (-1.0eV) exhibit adsorption energies within the -0.4eV to -1.0eV window, satisfying the energy criterion for stable and reversible adsorption.

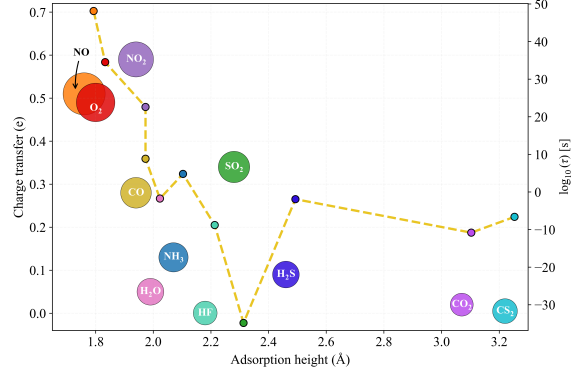
DOS analysis of the Mo-Ga₂O₂ ML reveals a similar behaviour to that of Zr-Ga₂O₂ ML, wherein the Fermi level penetrates the conduction band, indicating intrinsic metallic character (see Fig. 7b). Upon adsorption of H₂S, H₂O, and NH₃, the system retains its metallic character, indicating that the conductivity change relative to the Mo-Ga₂O₂ ML is not expected to be reliable enough for robust electrical detection (see Fig. S15 in SI). As a result, these molecules are not considered as target analytes for Mo-Ga₂O₂ ML.

The adsorption of CO (-1.24eV) falls in the borderline regime beyond the reversible sensing threshold yet below the -1.5eV irreversibility criterion. This indicates that the adsorption is too strong for practical surface recovery under ambient conditions, yet potentially amenable to external thermal annealing or UV photo-desorption treatment. CO adsorption drives the Fermi level out of the CB and induces a partially filled localized state near the CBE. The resulting excitation energy between this state and the CBE is approximately 0.164eV ($\approx 6k_B T$) (Fig. 7b). This is expected to reduce the electrical conductivity substantially, at room temperature. Therefore, the Mo-Ga₂O₂ ML acts as a sensing layer to CO molecule, but in O₂ controlled environment (discussed below).

In sharp contrast, NO (-3.58eV), O₂ (-2.77eV), and NO₂ (-2.06eV) exhibit adsorption energies far exceeding the -1.5eV threshold, accompanied by markedly low adsorption heights and substantial charge transfer. The corresponding values of E_{ads} , Q, H, and τ for all gas molecules on Mo-Ga₂O₂ are summarized in Fig. 8. The DOS remains largely unperturbed upon the adsorption of O₂, thereby suggesting negligible modification

Molecule	E_{ads} (eV)	H (Å)	q (e)	τ (s)
NH ₃	-1.00	2.07	-0.13	6.30×10^4
NO	-3.58	1.76	0.51	1.38×10^{48}
SO ₂	1.36	2.28	0.34	1.42×10^{-35}
O ₂	-2.77	1.80	0.49	3.42×10^{34}
NO ₂	-2.06	1.94	0.59	4.04×10^{22}
H ₂ S	-0.60	2.46	-0.09	1.20×10^{-2}
H ₂ O	-0.61	1.99	-0.05	1.77×10^{-2}
CO	-1.24	1.94	0.28	6.78×10^8
CO ₂	-0.07	3.07	0.02	1.50×10^{-11}
CS ₂	-0.32	3.22	0.005	2.38×10^{-7}
HF	-0.19	2.18	-0.0005	1.56×10^{-9}

(a)



(b)

Figure 8: (a) Table IV: Adsorption parameters of the investigated gas molecules on the Mo-Ga₂O₂ ML, including adsorption energy (E_{ads}), adsorption height (H), charge transfer (q), and recovery time (τ). (b) Graphical summary of the adsorption characteristics of gas molecules on the Mo-Ga₂O₂ monolayer. The centers of the larger bubbles are referenced to the X and primary Y-axes, representing the adsorption height and charge transfer, respectively. The area of each bubble is proportional to the magnitude of the adsorption energy. The smaller markers linked by the dashed line indicate the corresponding recovery times, referenced to the secondary Y-axis. Recovery times are reported on a logarithmic scale.

of the electrical conductivity. On the contrary, the adsorption of NO and NO₂ shifts the Fermi level out of the energy bands, giving rise to electron excitation energy of 0.81eV and 0.012eV, respectively (Fig. S15 in the SI). While these changes are expected to significantly suppress the conductivity, the exceptionally strong adsorption energies of these molecules suggest that scavenging behavior would dominate over reusable sensing capability. Consequently, the Mo-Ga₂O₂ ML appears more suitable for molecular scavenging applications toward NO, O₂, and NO₂.

3.4 Ag Substitution

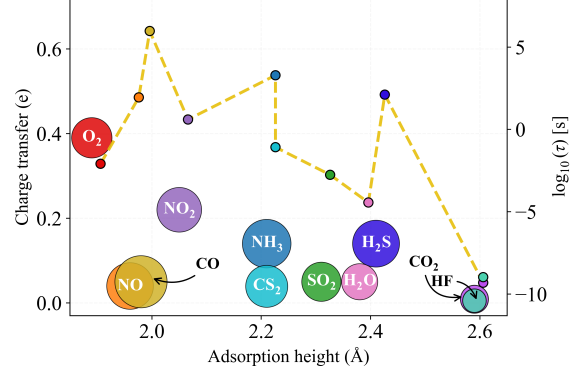
For the Ag-substituted ML (Ag-Ga₂O₂), based on the values of the adsorption energies, CO₂ ($E_{ads} = -0.16eV$) and HF ($-0.18eV$) are characterized by weak adsorption, as their adsorption energies lie above $-0.4eV$. Consequently, neither molecule satisfies the adsorption criterion adopted for practical gas sensing, and therefore their DOS are not analyzed further.

In contrast, molecules such as NH₃ ($E_{ads} = -0.91eV$), NO ($-0.83eV$), SO₂ ($-0.55eV$), NO₂ ($-0.75eV$), H₂S ($-0.84eV$), CS₂ ($-0.65eV$), CO ($-1.07eV$) along with the ambient species H₂O ($-0.45eV$) and O₂ ($-0.59eV$), exhibit comparatively stronger adsorption with E_{ads} lying within the favorable adsorption window. The values of E_{ads} , Q, H and τ are given in Fig. 9.

The DOS of Ag-Ga₂O₂ ML exhibits an induced localized filled state located approximately 1.17eV below the CBE (see Fig. 10). Upon adsorption of NH₃, CS₂, H₂S, and H₂O, the corresponding electron excitation energies remain largely unchanged, with values of approximately 1.017eV, 1.17eV, 1.22eV and 1.08eV, respectively (see Fig. S17 in SI). Such minor variations in the transition gaps are not expected to induce appreciable changes in the conductivity of the Ag-Ga₂O₂ ML, thereby yielding no meaningful conductometric response. In the light of this, we calculate the adsorption induced conductivity change factor (χ) to gauge the factor by which the conductivity changes upon adsorption of the molecules [11, 17, 26]. The expression for χ and details of its calculation are provided in Section 7.1 of SI. We note that although there is reasonable modulation in χ (Table 2), the large electron excitation energy of $-1.17eV$ keeps the baseline conductivity of Ag-Ga₂O₂ small. Hence, the change in χ maybe difficult to detect and prone to modulation due to other issues. Thus, these molecules remain largely invisible and are not expected to produce appreciable and reliable conductometric change in all these four cases. Consequently, these molecules are not considered

Molecule	E_{ads} (eV)	H (Å)	q (e)	τ (s)
NH ₃	-0.91	2.21	0.14	1.94×10^3
NO	-0.83	1.96	0.04	8.78×10^1
SO ₂	-0.55	2.31	0.05	1.74×10^{-3}
O ₂	-0.59	1.89	0.39	8.16×10^{-3}
NO ₂	-0.75	2.05	0.22	3.98×10^0
H ₂ S	-0.84	2.41	0.14	1.29×10^2
H ₂ O	-0.45	2.38	0.05	3.63×10^{-5}
CO	-1.07	1.98	0.05	9.45×10^5
CO ₂	-0.16	2.59	0.009	4.87×10^{-10}
CS ₂	-0.65	2.21	0.04	8.31×10^{-2}
HF	-0.18	2.59	0.005	1.06×10^{-9}

(a)



(b)

Figure 9: (a) Table V: Adsorption parameters of the investigated gas molecules on the Ag-Ga₂O₂ ML, including adsorption energy (E_{ads}), adsorption height (H), charge transfer (q), and recovery time (τ). (b) Graphical summary of the adsorption characteristics of gas molecules on the Ag-Ga₂O₂ monolayer. The centers of the larger bubbles are referenced to the X and primary Y-axes, representing the adsorption height and charge transfer, respectively. The area of each bubble is proportional to the magnitude of the adsorption energy. The smaller markers linked by the dashed line indicate the corresponding recovery times, referenced to the secondary Y-axis. Recovery times are reported on a logarithmic scale.

suitable target analytes for reusable sensing on the Ag-Ga₂O₂ platform.

CO and SO₂ adsorption modify the electronic structure of Ag-Ga₂O₂ by increasing the associated excitation energy. The electron excitation energy increases from approximately $1.17eV$ in the Ag-Ga₂O₂ ML to $1.32eV$ and $1.30eV$ upon CO and SO₂ adsorption, respectively. Although this increase is expected to suppress the conductivity, the relatively large excitation energy already present in the Ag-Ga₂O₂ limits the magnitude of the adsorption-induced conductivity change. Consequently, the resulting conductometric response is expected to be weak and may be difficult to resolve reliably in a simple resistive sensing setup. Consistent with this interpretation, the calculated χ values are of the order of 10^{-2} , indicating conductivity suppression but not necessarily a practically robust sensing signal. Therefore, these molecules cannot be considered as target analytes for Ag-Ga₂O₂ ML.

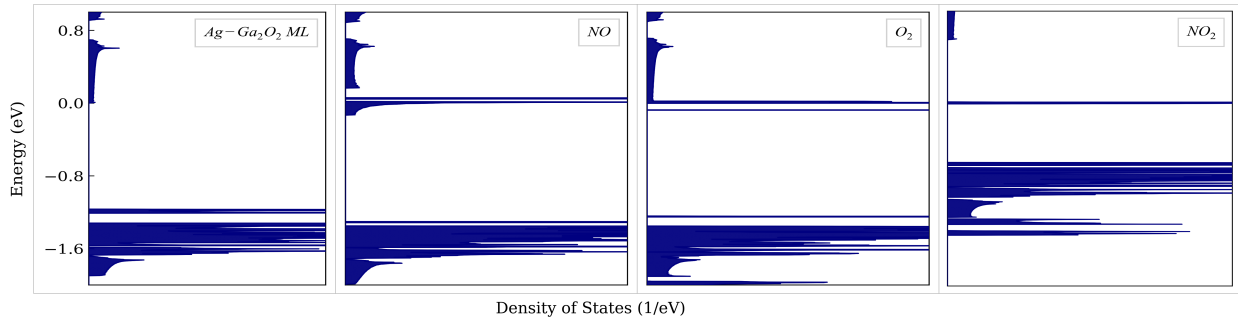


Figure 10: Total DOS of the Ag-Ga₂O₂ ML and upon adsorption of target gas molecules. The Fermi level is pinned at $0eV$ in all the panels.

In sharp contrast, NO ($E_{ads} = -0.83eV$) adsorption induces a qualitatively distinct electronic response (see Fig. 10). The adsorption of NO induces a partially filled state in close proximity to the CBE. This results in reducing the transition gap to approximately $0.14eV$ ($\approx 6k_B T$ at $T = 300K$) drastically. The proximity of this state to the conduction band substantially lowers the carrier excitation threshold, producing an

eight-order-of-magnitude enhancement in χ relative to the Ag-Ga₂O₂ ML. The resulting conductivity surge upon NO adsorption renders the Ag-Ga₂O₂ ML a highly sensitive platform for the resistive detection of NO in ambient conditions. Similarly, NO₂ ($E_{ads} = -0.75eV$) adsorption introduces a partially filled state in the vicinity of the Fermi level, located approximately $0.67eV$ ($\approx 26k_B T$ at $T = 300K$) below the CBE. Although larger than the corresponding gap in the NO-adsorbed system, this excitation energy gap remains substantially smaller than that of the Ag-Ga₂O₂ ML and is therefore expected to enhance the conductivity. This behaviour is consistent with the calculated value of χ , which increases by approximately four orders of magnitude upon NO₂ adsorption. Accordingly, both NO and NO₂ emerge as promising target analytes for reusable sensing on the Ag-Ga₂O₂ ML.

Analogous to NO, adsorption of O₂ ($E_{ads} = -0.59eV$) on the Ag-Ga₂O₂ ML induces a localized filled state at approximately $0.07eV$ ($\approx 3k_B T$ at $T = 300K$) below CBE. This near-edge state drives an approximately nine-order-of-magnitude enhancement in χ . Such a substantial enhancement signifies a pronounced increase in electrical conductivity upon O₂ adsorption, comparable to that observed for NO. However, given that O₂ is an ubiquitous constituent of ambient air, such binding and conductometric change with O₂ adsorption, raises a practical concern: under atmospheric conditions, O₂ molecules would competitively occupy the available adsorption sites, effectively passivating the sensor surface and suppressing its response toward other target analytes. This limitation, however, simultaneously defines a compelling niche for the Ag-Ga₂O₂ ML as a selective O₂ sensor. In oxygen-restricted or controlled-atmosphere environments such as inert-gas gloveboxes, ultra-high vacuum chambers, or hermetically sealed systems used for sensitive physical or chemical experiments, even trace quantities of O₂ represent a critical contamination hazard. The pronounced conductometric response of the Ag-Ga₂O₂ ML to O₂, combined with its suitable adsorption energy, positions it as a sensitive and reliable platform for detecting O₂ ingress in such environments, where its cross-sensitivity toward other analytes becomes operationally irrelevant.

Table 2: Calculated Adsorption-Induced Conductivity Change Factor (χ) for all favorably adsorbed gas molecules on the Ag-Ga₂O₂ ML.

Molecules	Ag Sub
NH ₃	17.84
NO	3.62×10^8
SO ₂	7.48×10^{-2}
O ₂	1.60×10^9
NO ₂	1.46×10^4
H ₂ S	0.35
H ₂ O	6.40
CO	5.08×10^{-2}
CS ₂	0.92

Selectivity Analysis for NO and NO₂ under realistic atmospheric conditions: Although NO detection may be viable in inert environments, its detection under ambient conditions needs to be analysed due to competition with O₂ for active adsorption sites. For practical detection of NO, the occupancy probability of an active site should be greater or comparable to that of O₂ or other ambient gases. To assess the practical viability of NO detection under ambient conditions, adsorption site occupancy probabilities were computed using a grand canonical adsorption model (Section 3.1, Eq. S3, SI) under realistic atmospheric conditions i.e. NO at 25 ppm, O₂ at 21%, alongside N₂ (79%), H₂O (5000 ppm), and CO₂ (400 ppm) at 1 atm total pressure, using DFT-calculated adsorption energies [64]. The resulting occupancy probabilities as a function of temperature and NO concentration are shown in Section 7.2.1, Fig. S21 in SI.

At 300 K, NO exhibits a site occupancy probability of approximately 55.7%, despite its concentration being roughly 840 times lower than that of O₂. This counterintuitive result is a direct consequence of NO’s stronger E_{ads} ($-0.83eV$) relative to O₂ ($-0.59eV$). It should be noted that this advantage is sustained around room temperatures but erodes with increasing temperature. At 400 K, O₂ occupancy probability rises to 79% while NO falls to 12%, and above 500 K empty sites begin to dominate as adsorption weakens exponentially.

The concentration variation at 300 K identifies a crossover point at approximately 20 ppm below which O₂ dominates site occupancy over NO. Since 25 ppm represents a widely adopted regulatory exposure threshold for NO [65, 66], the sensor operates precisely within the practically relevant detection window under ambient conditions.

The above results indicate that, at or near room temperature, NO (at 25 ppm) and O₂ (at 21%) would occupy the active sites with equal probabilities. Consequently, in the absence of NO, the adsorption sites are expected to be predominantly occupied by O₂. However, upon exposure to NO at concentrations of 20–25 ppm, which is the permissible exposure limit (PEL) for NO [65, 66], about half of these sites becomes occupied by NO at 300K. Therefore, practical NO detection under ambient conditions relies on the existence of a discernible conductometric difference between the O₂-adsorbed ML and the co-adsorbed O₂/NO ML. To assess this possibility, it is necessary to examine the electronic structure of the monolayer under simultaneous adsorption of O₂ and NO and evaluate whether the resulting conductance modulation remains sufficiently distinct for reliable NO detection in ambient environments. Hence, to further investigate the practical implications of O₂'s strong conductometric response under ambient conditions, a DFT simulation was performed by placing both O₂ and NO simultaneously on an 8×4×1 Ga₂O₂ supercell incorporating two Ag substitution sites, one for each molecule with sufficient intermolecular separation to preclude direct molecule-molecule interaction (see Section 7.2, Fig. S19 in SI). The resulting DOS reveals a qualitatively significant departure from that of the isolated O₂ case: the localized state previously observed at the CBE is absent, and instead a partially filled localised state emerges with the excitation energy of $\approx 0.22eV$, closely mirroring the electronic signature of isolated NO adsorption (see Section 7.2, Fig. S20 in SI). Crucially, the suppression of the O₂ induced state at the CBE in the presence of NO is a favorable outcome from a sensing perspective. Hence, it is expected that in the ambient environment around the room temperature; Ag-Ga₂O₂ ML will show large conductivity due to adsorption of sufficient O₂ molecule. However, once exposed to NO, the conductivity would drop appreciably due to the increase in the electron excitation energy to 0.22eV. It should be noted that although NO adsorption increases the electron excitation energy to 0.22eV, this value corresponds to only $\approx 9k_B T$ at room temperature. Therefore, while a measurable reduction in conductivity is expected, the conductivity is unlikely to be suppressed by several orders of magnitude.

Collectively, both the site occupancy analysis and co-adsorption DOS consistently establish that the Ag-Ga₂O₂ ML retains selective sensitivity toward NO under ambient conditions, with NO's stronger adsorption energy serving as the decisive factor in both surface site competition and electronic structure determination.

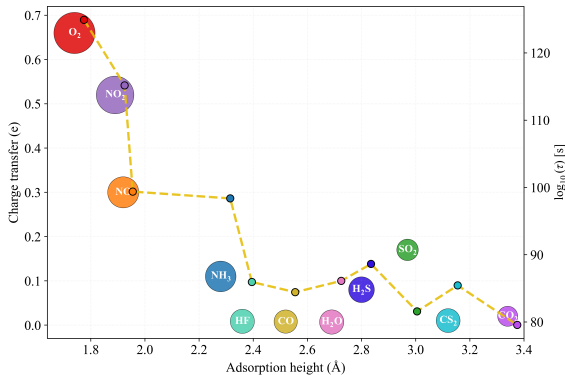
Assessment of NO₂ sensing under ambient conditions: Similar to NO, the practical viability of NO₂ sensing under ambient conditions was evaluated by computing occupancy probabilities for active sites. The concentration of NO₂ was taken as 25 ppm and 40 ppm. Despite the favorable adsorption energy of NO₂ ($-0.75eV$), the substantially higher concentration of O₂ results in preferential occupation of the active sites by O₂. At 25 ppm of NO₂, its calculated site occupancy probability is $\sim 19\%$ while for O₂, it is $\sim 81\%$. Increasing the NO₂ concentration to 40 ppm raises the NO₂ occupancy to only $\sim 27\%$. In fact, the calculated crossover concentration, at which NO₂ and O₂ exhibit comparable site occupancies, is approximately 9400 ppm, far exceeding environmentally relevant NO₂ levels. This further confirms that competitive adsorption by O₂ is expected to suppress practical NO₂ sensing under ambient conditions. Nevertheless, the favorable adsorption energy and conductometric response of NO₂ suggest that its detection may still be feasible under O₂ controlled or O₂-deficient environments, where competitive occupation by atmospheric O₂ is substantially reduced. Similar to the NO co-adsorption case, a simulation was performed by simultaneously placing O₂ and NO₂ on an 8×4×1 Ga₂O₂ supercell containing two Ag substitution sites, one for each molecule, while maintaining sufficient intermolecular separation to eliminate direct molecule-molecule interactions (see Section 7.3, Fig. S22 in SI). The resulting DOS exhibits a qualitatively distinct electronic structure compared to the isolated O₂-adsorbed system. In particular, the localized state previously located at the CBE is no longer present. Instead, a partially filled state emerges, giving rise to an excitation energy of approximately 0.84eV to CB. Notably, this electronic signature closely resembles that of the isolated NO₂-adsorbed system (see Section 7.3, Fig. S23 in SI), suggesting that despite the dominant occupancy of O₂, the electronic response of the co-adsorbed configuration is governed primarily by the presence of NO₂. The detailed occupancy probability calculations and co-adsorption analysis are provided in Section 7.3

of SI, respectively. Nevertheless, despite its intrinsic selectivity toward NO_2 , competitive occupation by atmospheric O_2 limits the practical viability of the Ag- Ga_2O_3 ML for ambient NO_2 sensing.

3.5 Ti and Pt Substitution

Ti-substituted System: The Ti-substituted ML ($\text{Ti-Ga}_2\text{O}_3$) exhibits the most aggressive adsorption characteristics among all substitutional configurations examined in this study. All eleven analytes display adsorption energies far exceeding the -1.5eV irreversibility threshold, ranging from a maximum of -5.45eV for CO_2 to a minimum of -8.15eV for O_2 , with very prolonged recovery times, (see Fig. 11). This universally extreme binding behavior unambiguously classifies the Ti- Ga_2O_3 ML as a broad-spectrum chemical scavenger, capable of permanently immobilizing all target analytes regardless of their chemical nature or molecular polarity.

Molecule	E_{ads} (eV)	H (Å)	q (e)	τ (s)
NH_3	-6.57	2.28	0.11	2.35×10^{98}
NO	-6.63	1.92	0.30	2.39×10^{99}
SO_2	-5.57	2.97	0.17	3.73×10^{81}
O_2	-8.15	1.74	0.66	8.20×10^{124}
NO_2	-7.57	1.89	0.52	1.48×10^{115}
H_2S	-5.99	2.80	0.08	4.24×10^{88}
H_2O	-5.84	2.69	0.007	1.28×10^{86}
CO	-5.74	2.52	0.008	2.68×10^{84}
CO_2	-5.45	3.34	0.02	3.60×10^{79}
CS_2	-5.80	3.12	0.01	2.73×10^{85}
HF	-5.83	2.36	0.008	8.70×10^{85}



(a)

(b)

Figure 11: (a) Table VI: Adsorption parameters of the investigated gas molecules on the Ti- Ga_2O_3 ML, including adsorption energy (E_{ads}), adsorption height (H), charge transfer (q), and recovery time (τ). (b) Graphical summary of the adsorption characteristics of gas molecules on the Ti- Ga_2O_3 monolayer. The centers of the larger bubbles are referenced to the X and primary Y-axes, representing the adsorption height and charge transfer, respectively. The area of each bubble is proportional to the magnitude of the adsorption energy. The smaller markers linked by the dashed line indicate the corresponding recovery times, referenced to the secondary Y-axis. Recovery times are reported on a logarithmic scale.

Examination of adsorption heights and charge transfer reveals two dominant interaction characteristics at the Ti site. The first is observed for O_2 ($H=1.74\text{Å}$, $Q=0.66e$), NO_2 (1.89Å , $0.52e$), and NO (1.92Å , $0.30e$), where low adsorption heights and substantial charge transfer indicate strong adsorption accompanied by significant electron-density transfer from the Ti-substituted surface to the adsorbed molecules. The significant charge transfer upon adsorption is expected to strengthen the electrostatic attraction between the adsorbate and the Ti-substituted surface, which is reflected in the relatively short adsorption distances. The relaxed geometries further exhibit noticeable molecular reorientation and, in selected cases, mild structural distortion consistent with chemisorptive behaviour (see Fig. S19 in SI).

The second interaction characteristic is observed for H_2O , CO , CO_2 , CS_2 , and HF , which exhibit negligible net charge transfer ($\leq 0.02e$) despite very strong adsorption energies (-5.45 to -5.84eV). Together with the relaxed geometries, this indicates that their binding is not governed by net ionic charge transfer, but rather by strong covalent-type interaction between molecular orbitals and Ti d -states. The low net charge transfer may arise from compensated donation and back-donation processes, leading to substantial charge redistribution without a large net electron transfer [11]. NH_3 , SO_2 , and H_2S exhibit intermediate behavior, with moderate charge transfer ($0.11e$, $0.17e$, and $0.08e$, respectively), suggesting a mixed nature of interaction.

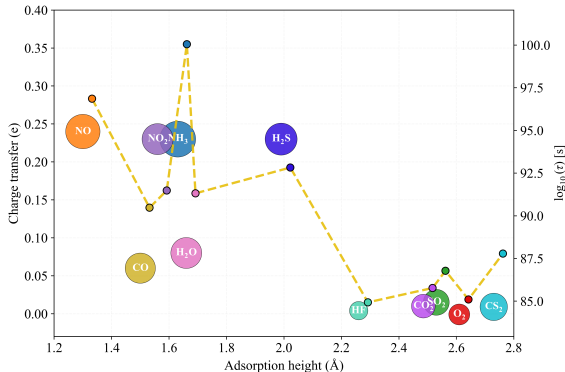
Given the universally irreversible adsorption nature, DOS analysis is not pursued for the Ti- Ga_2O_3 ML. The

extreme adsorption energies across all eleven gas molecules spanning ambient, toxic, and corrosive species alike unambiguously establish its role as a broad-spectrum chemical scavenger. Hence, the potential utility of Ti-Ga₂O₂ ML may lie in creating and maintaining chemically inert or ultra-clean environments where complete removal of gas-phase species is desired.

Pt-substituted System: The Pt-substituted ML (Pt-Ga₂O₂) mirrors same behaviour as the Ti-Ga₂O₂ ML in its broad-spectrum scavenging behavior, with all analytes exhibiting adsorption energies ranging from a maximum of $-5.77eV$ to a minimum of $-6.67eV$ for HF and NH₃ respectively, and hence, extremely long recovery times, (see Fig. 12). This firmly establishes irreversible molecular capture across the entire panel of target gases. However, the underlying adsorption mechanism differs fundamentally from that of the Ti site.

Molecule	E_{ads} (eV)	H (Å)	q (e)	τ (s)
NH ₃	-6.67	1.63	-0.23	1.12×10^{100}
NO	-6.48	1.30	-0.24	7.23×10^{96}
SO ₂	-5.88	2.56	0.005	6.02×10^{86}
O ₂	-5.78	2.58	-0.005	1.26×10^{85}
NO ₂	-6.16	1.56	0.23	3.04×10^{91}
H ₂ S	-6.24	1.99	-0.23	6.72×10^{92}
H ₂ O	-6.15	1.66	-0.08	2.07×10^{91}
CO	-6.10	1.50	-0.06	2.99×10^{90}
CO ₂	-5.82	2.51	0.01	5.91×10^{85}
CS ₂	-5.94	2.72	-0.009	6.13×10^{87}
HF	-5.77	2.26	0.004	8.55×10^{84}

(a)



(b)

Figure 12: (a) Table VII: Adsorption parameters of the investigated gas molecules on the Pt-Ga₂O₂ ML, including adsorption energy (E_{ads}), adsorption height (H), charge transfer (q), and recovery time (τ). (b) Graphical summary of the adsorption characteristics of gas molecules on the Pt-Ga₂O₂ monolayer. The centers of the larger bubbles are referenced to the X and primary Y-axes, representing the adsorption height and charge transfer, respectively. The area of each bubble is proportional to the magnitude of the adsorption energy. The smaller markers linked by the dashed line indicate the corresponding recovery times, referenced to the secondary Y-axis. Recovery times are reported on a logarithmic scale.

Unlike Ti, where two distinct interaction characteristics were identified through substantial charge transfer values, the Pt site is characterized by near-universally low charge transfer magnitudes across all molecules, with values rarely exceeding $0.1e$. This suggests that the binding on the Pt site is predominantly covalent in character, driven by orbital hybridization between the adsorbate and the Pt d-states rather than ionic charge redistribution. The adsorption heights, ranging from 1.30\AA for NO to 2.72\AA for CS₂, are consistent with strong orbital overlap supporting this hybridization-dominated picture. The Pt-Ga₂O₂ ML is therefore also conclusively identified as a broad-spectrum chemical scavenger, with the distinction that its capture mechanism is predominantly covalent and hybridization-driven.

Section 11 of SI provides a comparative summary of literature-reported adsorption energies and recovery times for NO, NO₂, O₂, CO, and CO₂ on various 2D materials. The complete adsorption-energy landscape of the investigated TM-substituted Ga₂O₂ monolayers is presented as a heat map in Fig. S26 in SI. The resulting sensing and scavenging functionalities, classified according to the adopted screening criterion, are summarized in Fig. 13.

4 Conclusion

In summary, this work presents a systematic first-principles investigation of transition metal substituted Ga₂O₂ monolayer as platforms for gas sensing and molecular scavenging, motivated by the limited analyte

Dopants Molecules	Pd	Zn	Zr	Mo	Ag	Ti	Pt
NH₃	-	-	-	-	-	S c a v e n g i n g	S c a v e n g i n g
NO	Assisted Recovery	Reusable	Assisted Recovery	Scavenging	Reusable		
SO₂	-	-	-	-	-		
O₂	-	Reusable	Scavenging	Scavenging	Reusable		
NO₂	Reusable	Assisted Recovery	Scavenging	Scavenging	Reusable		
H₂S	-	-	-	-	-		
H₂O	-	-	-	-	-		
CO	-	-	-	Assisted Recovery	-		
CO₂	Reusable	-	-	-	-		
CS₂	-	-	-	-	-		
HF	-	-	-	-	-		

Figure 13: Summary of the sensing and scavenging characteristics of the investigated transition metal-substituted Ga₂O₂ monolayer toward the studied gas molecules. The color coding identifies reusable sensing applications (green), sensing applications requiring external assistance for recovery (blue), and scavengers exhibiting effectively irreversible adsorption (pink). Blank cells correspond to systems that do not exhibit practically relevant sensing or scavenging performance under the adopted screening criteria.

range and absence of irreversible capture capability in the pristine Ga₂O₂ surface. Across seven dopant species and eleven target gas molecules, substitutional doping is shown to dramatically expand the functional landscape of the Ga₂O₂ ML, from selective room-temperature resistive sensing to broad-spectrum irreversible molecular capture. Pd-Ga₂O₂ supports reusable sensing of NO₂ and CO₂, with NO sensing remaining accessible through assisted-recovery operation. Zn-Ga₂O₂ further expands the sensing functionality of the substituted ML, enabling reusable detection of NO and O₂, while NO₂ lies within the assisted-recovery regime. Beyond these reusable sensing platforms, Zr-Ga₂O₂ exhibits sensing potential toward NO within the assisted-recovery regime, while selectively scavenging O₂ and NO₂. In addition, Mo-Ga₂O₂ displays analogous sensing behavior toward CO and additionally functions as a selective scavenger for NO, NO₂, and O₂. Among all investigated systems, Ag-Ga₂O₂ produces the most pronounced conductometric response, yielding an approximately eight and nine -order-of-magnitude enhancement in electrical conductivity upon NO and O₂ adsorption at room temperature. In addition, Ag-Ga₂O₂ exhibits reusable sensing potential toward O₂ and NO₂. Additional analysis of selectivity in the ambient environment demonstrate that Pd-Ga₂O₂ and Ag-Ga₂O₂ remain selective towards NO while Zn-Ga₂O₂ remains selective towards NO₂ under normal atmospheric conditions. At the extreme end, Ti and Pt drive universally irreversible molecular capture, a capability that eluded the pristine Ga₂O₂ surface entirely. Beyond the scope of the present work, the exploration of additional dopant species and the effects of adatom functionalization remain promising avenues for further expanding the functional versatility of the Ga₂O₂ monolayer. These directions remain the subject of future investigation.

Acknowledgements

A.A.H. acknowledges the Ministry of Education, Govt. of India, for the Prime Minister’s Research Fellowship (PMRF). The authors acknowledge National Supercomputing Mission (NSM) for providing computing resources of ‘PARAM Shakti’ at IIT Kharagpur, implemented by C-DAC and supported by the Ministry of Electronics and Information Technology (MeitY) and Department of Science and Technology (DST), Government of India.

Supporting information

Supplementary Information (SI) available: AIMD plots, Optimized adsorption configurations, DOS plots, charge density difference isosurfaces, conductivity change factor (χ) calculations, competitive adsorption analysis, and additional computational details.

References

- [1] Z. Zhao, Y. Yong, Q. Zhou, Y. Kuang, and X. Li, “Gas-sensing properties of the SiC monolayer and bilayer: a density functional theory study,” *ACS omega*, vol. 5, no. 21, pp. 12 364–12 373, 2020. [Online]. Available: <https://doi.org/10.1021/acsomega.0c01084>
- [2] L. Zhang, K. Khan, J. Zou, H. Zhang, and Y. Li, “Recent advances in emerging 2D material-based gas sensors: potential in disease diagnosis,” *Advanced Materials Interfaces*, vol. 6, no. 22, p. 1901329, 2019. [Online]. Available: <https://doi.org/10.1002/admi.201901329>
- [3] D. J. Buckley, N. C. Black, E. G. Castanon, C. Melios, M. Hardman, and O. Kazakova, “Frontiers of graphene and 2D material-based gas sensors for environmental monitoring,” *2D Materials*, vol. 7, no. 3, p. 032002, 2020. [Online]. Available: <https://doi.org/10.1088/2053-1583/ab7bc5>
- [4] B. Wang, Y. Gu, L. Chen, L. Ji, H. Zhu, and Q. Sun, “Gas sensing devices based on two-dimensional materials: a review,” *Nanotechnology*, vol. 33, no. 25, p. 252001, 2022. [Online]. Available: <https://doi.org/10.1088/1361-6528/ac5df5>
- [5] T. Vincent, J. Liang, S. Singh, E. G. Castanon, X. Zhang, A. McCreary, D. Jariwala, O. Kazakova, and Z. Y. Al Balushi, “Opportunities in electrically tunable 2D materials beyond graphene: Recent progress and future outlook,” *Applied Physics Reviews*, vol. 8, no. 4, 2021. [Online]. Available: <https://doi.org/10.1063/5.0051394>
- [6] A. Chaves, J. G. Azadani, H. Alsalman, D. Da Costa, R. Frisenda, A. Chaves, S. H. Song, Y. D. Kim, D. He, J. Zhou *et al.*, “Bandgap engineering of two-dimensional semiconductor materials,” *npj 2D Materials and Applications*, vol. 4, no. 1, p. 29, 2020. [Online]. Available: <https://doi.org/10.1038/s41699-020-00162-4>
- [7] L. Yuan, D. Xidong, S. Hyeon-Jin, P. Seongjun, H. Yu, and D. Xiangfeng, “Promises and prospects of two-dimensional transistors,” *Nature*, vol. 591, no. 7848, pp. 43–53, 2021. [Online]. Available: <https://doi.org/10.1038/s41586-021-03339-z>
- [8] C. Huyghebaert, T. Schram, Q. Smets, T. Kumar Agarwal, D. Verreck, S. Brems, A. Phommahaxay, D. Chiappe, S. El Kazzi, C. Lockhart de la Rosa, G. Arutchelvan, D. Cott, J. Ludwig, A. Gaur, S. Sutar, A. Leonhardt, D. Marinov, D. Lin, M. Caymax, I. Asselberghs, G. Pourtois, and I. Radu, “2d materials: roadmap to cmos integration,” in *2018 IEEE International Electron Devices Meeting (IEDM)*, 2018, pp. 22.1.1–22.1.4. [Online]. Available: <https://doi.org/10.1109/IEDM.2018.8614679>
- [9] F. Schedin, A. K. Geim, S. V. Morozov, E. W. Hill, P. Blake, M. I. Katsnelson, and K. S. Novoselov, “Detection of individual gas molecules adsorbed on graphene,” *Nature materials*, vol. 6, no. 9, pp. 652–655, 2007. [Online]. Available: <https://doi.org/10.1038/nmat1967>

- [10] M. J. Szary, “First-principles design rules for selective room-temperature gas sensing in transition-metal-doped MoS_2 ,” *ACS Applied Materials & Interfaces*, vol. 18, no. 8, pp. 12 938–12 948, 2026. [Online]. Available: <https://doi.org/10.1021/acsami.5c23014>
- [11] B. A. Kalwar, W. Fangzong, A. M. Soomro, M. R. Naich, M. H. Saeed, and I. Ahmed, “Highly sensitive work function type room temperature gas sensor based on ti doped hbn monolayer for sensing CO_2 , CO, H_2S , HF and NO. a DFT study,” *RSC advances*, vol. 12, no. 53, pp. 34 185–34 199, 2022. [Online]. Available: <https://doi.org/10.1039/D2RA06307G>
- [12] H. Ahmad, M. Khan, G. A. Shazly, M. Bourhia, H. U. Rehman, Y. Liu, and F. Wang, “First-principles investigation of Sc and Ti-decorated hBN monolayers as adsorbents and gas sensors for SF_6 decomposition products,” *Chemical Physics*, vol. 595, p. 112708, 2025. [Online]. Available: <https://doi.org/10.1016/j.chemphys.2025.112708>
- [13] J. Wu, B. Wang, Y. Wei, R. Yang, and M. Dresselhaus, “Mechanics and mechanically tunable band gap in single-layer hexagonal boron-nitride,” *Materials Research Letters*, vol. 1, no. 4, pp. 200–206, 2013. [Online]. Available: <https://doi.org/10.1080/21663831.2013.824516>
- [14] J. Zhao, X. Huang, Y. Yin, Y. Liao, H. Mo, Q. Qian, Y. Guo, X. Chen, Z. Zhang, and M. Hua, “Two-Dimensional Gallium Oxide Monolayer for Gas-Sensing Application,” *The Journal of Physical Chemistry Letters*, vol. 12, no. 24, pp. 5813–5820, 2021. [Online]. Available: <https://doi.org/10.1021/acs.jpcclett.1c01393>
- [15] R. Al Nahean, M. Bala, M. T. Rahman, and M. R. Firoz, “Tailoring pt-loaded MoS_2/SnO_2 heterostructures for high-sensitivity room-temperature ammonia detection: a DFT and COMSOL analysis,” *Journal of Materials Chemistry A*, vol. 14, no. 19, pp. 11 689–11 709, 2026. [Online]. Available: <https://doi.org/10.1039/D5TA07648J>
- [16] Y. Zhang, Z. Zhang, G. Lv, Y. Zhang, J. Chen, Y. Luo, and G. Duan, “Ultrafast-response H_2S MEMS gas sensor based on double phase In_2O_3 monolayer particle film,” *Sensors and Actuators B: Chemical*, vol. 412, p. 135787, 2024. [Online]. Available: <https://doi.org/10.1016/j.snb.2024.135787>
- [17] A. A. Haque, S. G. Dhongade, and A. Singha, “Gas sensing properties of a novel indium oxide monolayer: A first-principles study,” *ACS omega*, vol. 10, no. 50, pp. 62 116–62 125, 2025. [Online]. Available: <https://doi.org/10.1021/acsomega.5c09366>
- [18] Y. Hahn and A. Umar, *Metal Oxide Nanostructures and Their Applications*, ser. Metal Oxide Nanostructures and Their Applications. American Scientific Publishers, 2010. [Online]. Available: <https://books.google.co.in/books?id=LfhntwAACAAJ>
- [19] Y. Zeng, S. Lin, D. Gu, and X. Li, “Two-dimensional nanomaterials for gas sensing applications: The role of theoretical calculations,” *Nanomaterials*, vol. 8, no. 10, 2018. [Online]. Available: <https://www.mdpi.com/2079-4991/8/10/851>
- [20] L. Shao, X. Duan, Y. Li, F. Zeng, H. Ye, and P. Ding, “Two-dimensional Ga_2O_2 monolayer with tunable band gap and high hole mobility,” *Physical Chemistry Chemical Physics*, vol. 23, no. 1, pp. 666–673, 2021. [Online]. Available: <https://doi.org/10.1039/D0CP05171C>
- [21] S. Demirci, N. Avazl ı, E. Durgun, and S. Cahangirov, “Structural and electronic properties of monolayer group III monochalcogenides,” *Phys. Rev. B*, vol. 95, p. 115409, Mar 2017. [Online]. Available: <https://link.aps.org/doi/10.1103/PhysRevB.95.115409>
- [22] T. Li, Z. Jin, Y. Xu, J. Zou, L.-L. Wang, and L. Xu, “Z-scheme $MoSi_2N_4/GaO$ van der waals heterostructure for efficient photocatalytic water splitting,” *Molecular Catalysis*, vol. 592, p. 115718, 2026. [Online]. Available: <https://www.sciencedirect.com/science/article/pii/S2468823126000180>
- [23] L. Yang, J. Zhang, H. Tan, Z. Zhang, Y. Wu, and X. Wang, “Design of Sc_2CF_2/Ga_2O_2 direct Z-scheme Van der Waals heterojunction for highly efficient solar-driven water splitting,” *Computational and Theoretical Chemistry*, vol. 1263, p. 115899, 2026. [Online]. Available: <https://www.sciencedirect.com/science/article/pii/S2210271X26002434>

- [24] B. Al-Faqiri, M. Rashad, S. Al-Osaimi, A. Al-Ghamdi, F. A. Al-Shehri, M. M. Al-Belwi, S. Al-Ghamdi, and N. M. Shaalan, "Effect of Ga_2O_2 -graphene heterostructures on methyl blue degradation in wastewater," *Desalination and Water Treatment*, vol. 296, pp. 111–118, 2023. [Online]. Available: <https://doi.org/10.5004/dwt.2023.29632>
- [25] L. Liu, L. Xu, Q. Wang, Z. Jin, Y. Yang, Y. Li, L. Wang, and K. Dong, "Visible-Light-Driven Spontaneous Water Splitting in a 2D Janus WSSe/GaO Z-Scheme Heterostructure," *ChemPhysChem*, vol. 27, no. 8, p. e202500893, 2026. [Online]. Available: <https://chemistry-europe.onlinelibrary.wiley.com/doi/abs/10.1002/cphc.202500893>
- [26] A. A. Haque, S. G. Dhongade, and A. Singha, "Predictive analysis of gas sensing properties in a novel 2D gallium oxide phase," *IEEE Sensors Journal*, 2025. [Online]. Available: <https://doi.org/10.1109/JSEN.2025.3548153>
- [27] K. Zhang and J. Robinson, "Doping of two-dimensional semiconductors: A rapid review and outlook," *MRS Advances*, vol. 4, no. 51–52, p. 2743–2757, 2019. [Online]. Available: <https://doi.org/10.1557/adv.2019.391>
- [28] D. Han, W. Ming, H. Xu, S. Chen, D. Sun, and M.-H. Du, "Chemical trend of transition-metal doping in WSe_2 ," *Phys. Rev. Appl.*, vol. 12, p. 034038, Sep 2019. [Online]. Available: <https://link.aps.org/doi/10.1103/PhysRevApplied.12.034038>
- [29] P. Panigrahi *et al.*, "Elemental substitution of two-dimensional transition metal dichalcogenides for energy and sensing applications," *ACS Sensors*, vol. 4, pp. 2646–2660, 2019. [Online]. Available: <https://doi.org/10.1021/acssensors.9b01044>
- [30] D. Maity, R. Sharma, K. R. Sahoo, A. Lal, R. Arenal, and T. N. Narayanan, "Tuning the electronic structure of monolayer MoS_2 towards metal like via Vanadium doping," *Phys. Rev. Mater.*, vol. 8, p. 084002, Aug 2024. [Online]. Available: <https://link.aps.org/doi/10.1103/PhysRevMaterials.8.084002>
- [31] P. L. G. Moody and N. Anders, "A molecular perspective on the d-band model: Synergy between experiment and theory," *Topics in Catalysis*, vol. 57, no. 1, pp. 2–13, 2014. [Online]. Available: <https://doi.org/10.1007/s11244-013-0157-4>
- [32] L.-Y. Guo, S.-Y. Xia, Y. Tan, and Z. Huang, "Zr-doped h-BN monolayer: a high-sensitivity atmospheric pollutant-monitoring sensor," *Sensors*, vol. 22, no. 11, p. 4103, 2022. [Online]. Available: <https://doi.org/10.3390/s22114103>
- [33] A. Abdesselem, C. Siouani, S. Mahtout, and A. Alouache, "Hazardous gas adsorption on Zr-doped SiC monolayer: A density functional theory study," *Materials Science in Semiconductor Processing*, vol. 206, p. 110461, 2026. [Online]. Available: <https://doi.org/10.1016/j.mssp.2026.110461>
- [34] J. Su, X. Liu, H. Zhang, B. Zhao, and T. Shen, "Effect of metal (Zn and Co) doped/co-doped on $Ti_3C_2O_2$ MXene to NO gas sensing capability: a DFT study," *Micro and Nanostructures*, vol. 183, p. 207658, 2023. [Online]. Available: <https://doi.org/10.1016/j.micrna.2023.207658>
- [35] F. Mollaamin and M. Monajjemi, "Transition metal (X= Mn, Fe, Co, Ni, Cu, Zn)-doped graphene as gas sensor for CO_2 and NO_2 detection: A Molecular Modeling Framework by DFT Perspective," *Journal of Molecular Modeling*, vol. 29, no. 4, p. 119, 2023. [Online]. Available: <https://doi.org/10.1007/s00894-023-05526-3>
- [36] N. Cheghib, A.-G. Boudjahem, and M. Dardare, "First-principles study of the transition metal (Rh, Ru, Mo and Co)-doped GaN monolayers: Structural stability, electronic properties and potential for toxic gas detection," *Materials Science in Semiconductor Processing*, vol. 203, p. 110237, 2026. [Online]. Available: <https://doi.org/10.1016/j.mssp.2025.110237>
- [37] T. Akter, M. J. Islam, M. T. Rahman, and J. Islam, "Hazardous gas adsorption and sensing by pristine and Pd/Mo-decorated TiS_2 : a first-principles study," *RSC advances*, vol. 15, no. 53, pp. 45 081–45 098, 2025. [Online]. Available: <https://doi.org/10.1039/D5RA06850A>

- [38] L. Wang, W. Li, Y. Cai, P. Pan, J. Li, G. Bai, and J. Xu, “Characterization of Pt-or Pd-doped graphene based on density functional theory for H_2 gas sensor,” *Materials Research Express*, vol. 6, no. 9, p. 095603, 2019. [Online]. Available: <https://doi.org/10.1088/2053-1591/ab2dc0>
- [39] N. Viveka, C. Poornimadevi, C. P. Kala, and D. J. Thiruvadigal, “DFT insights into the gas sensing properties of light platinum group metal (Ru, Rh & Pd) doped $MoSe_2$ Monolayers,” *Surfaces and Interfaces*, vol. 66, p. 106579, 2025. [Online]. Available: <https://www.sciencedirect.com/science/article/pii/S2468023025008363>
- [40] L.-Y. Guo, S.-Y. Xia, H. Sun, C.-H. Li, Y. Long, C. Zhu, Y. Gui, Z. Huang, and J. Li, “A DFT study of the Ag-doped h-BN monolayer for harmful gases (NO_2 , SO_2F_2 , and NO),” *Surfaces and Interfaces*, vol. 32, p. 102113, 2022. [Online]. Available: <https://doi.org/10.1016/j.surfin.2022.102113>
- [41] H. Zhang, M. Wang, X. Cheng, S. Chen, Y. Yang, B. Yu, W. Qiu, and W. Zeng, “A DFT study of transition metal (Ag, Ni) doped WS_2 monolayer as promising sensing materials for SF_6/N_2 decomposition gases,” *Surface Science*, p. 122990, 2026. [Online]. Available: <https://doi.org/10.1016/j.susc.2026.122990>
- [42] D. Kong, B. Ma, L. Zhang, L. Yang, C. Li, C. Yin, K. Wu, and Y. Wang, “Metal (Au, Ag, Pt) Doping Effects on the Gas-Sensing Mechanism and Characteristics of Two-Dimensional WS_2 : A First-Principle,” *ACS Applied Electronic Materials*, vol. 6, no. 2, pp. 958–968, 2024. [Online]. Available: <https://doi.org/10.1021/acsaelm.3c01450>
- [43] D. Chen, X. Zhang, J. Tang, H. Cui, and Y. Li, “Noble metal (Pt or Au)-doped monolayer MoS_2 as a promising adsorbent and gas-sensing material to SO_2 , SOF_2 and SO_2F_2 : a DFT study,” *Applied Physics A*, vol. 124, no. 2, p. 194, 2018. [Online]. Available: <https://doi.org/10.1007/s00339-018-1629-y>
- [44] J. P. Perdew, K. Burke, and M. Ernzerhof, “Generalized gradient approximation made simple,” *Physical Review Letters*, vol. 77, no. 18, p. 3865, 1996. [Online]. Available: <https://doi.org/10.1103/PhysRevLett.77.3865>
- [45] G. Kresse and J. Furthmüller, “Efficiency of ab-initio total energy calculations for metals and semiconductors using a plane-wave basis set,” *Computational Materials Science*, vol. 6, no. 1, pp. 15–50, 1996. [Online]. Available: [https://doi.org/10.1016/0927-0256\(96\)00008-0](https://doi.org/10.1016/0927-0256(96)00008-0)
- [46] P. E. Blöchl, “Projector augmented-wave method,” *Physical review B*, vol. 50, no. 24, p. 17953, 1994. [Online]. Available: <https://doi.org/10.1103/PhysRevB.50.17953>
- [47] L. Goerigk, “A comprehensive overview of the DFT-D3 london-dispersion correction,” *Non-covalent interactions in quantum chemistry and physics*, pp. 195–219, 2017. [Online]. Available: <https://doi.org/10.1016/B978-0-12-809835-6.00007-4>
- [48] J. Witte, N. Mardirossian, J. B. Neaton, and M. Head-Gordon, “Assessing DFT-D3 damping functions across widely used density functionals: Can we do better?” *Journal of Chemical Theory and Computation*, vol. 13, no. 5, pp. 2043–2052, 2017. [Online]. Available: <https://doi.org/10.1021/acs.jctc.7b00176>
- [49] C. G. Van de Walle and J. Neugebauer, “First-principles calculations for defects and impurities: Applications to III-nitrides,” *Journal of applied physics*, vol. 95, no. 8, pp. 3851–3879, 2004. [Online]. Available: <https://doi.org/10.1063/1.1682673>
- [50] S. Zhang and J. E. Northrup, “Chemical potential dependence of defect formation energies in GaAs: Application to Ga self-diffusion,” *Physical review letters*, vol. 67, no. 17, p. 2339, 1991. [Online]. Available: <https://doi.org/10.1103/PhysRevLett.67.2339>
- [51] J. Rogal, S. V. Divinski, M. W. Finnis, A. Glensk, J. Neugebauer, J. H. Perepezko, S. Schuwalow, M. H. Sluiter, and B. Sundman, “Perspectives on point defect thermodynamics,” *physica status solidi (b)*, vol. 251, no. 1, pp. 97–129, 2014. [Online]. Available: <https://doi.org/10.1002/pssb.201350155>

- [52] S. Pearton, J. Yang, P. H. Cary, F. Ren, J. Kim, M. J. Tadjer, and M. A. Mastro, “A review of Ga_2O_3 materials, processing, and devices,” *Applied Physics Reviews*, vol. 5, no. 1, 2018. [Online]. Available: <https://doi.org/10.1063/1.5006941>
- [53] J. Y. Tsao, S. Chowdhury, M. A. Hollis, D. Jena, N. M. Johnson, K. A. Jones, R. J. Kaplar, S. Rajan, C. G. Van de Walle, E. Bellotti, C. L. Chua, R. Collazo, M. E. Coltrin, J. A. Cooper, K. R. Evans, S. Graham, T. A. Grotjohn, E. R. Heller, M. Higashiwaki, M. S. Islam, P. W. Juodawlkis, M. A. Khan, A. D. Koehler, J. H. Leach, U. K. Mishra, R. J. Nemanich, R. C. N. Pilawa-Podgurski, J. B. Shealy, Z. Sitar, M. J. Tadjer, A. F. Witulski, M. Wraback, and J. A. Simmons, “Ultrawide-bandgap semiconductors: Research opportunities and challenges,” *Advanced Electronic Materials*, vol. 4, no. 1, p. 1600501, 2018. [Online]. Available: <https://advanced.onlinelibrary.wiley.com/doi/abs/10.1002/aelm.201600501>
- [54] M. Higashiwaki and G. H. Jessen, “Guest editorial: The dawn of gallium oxide microelectronics,” *Applied Physics Letters*, vol. 112, no. 6, 2018. [Online]. Available: <https://doi.org/10.1063/1.5017845>
- [55] R. Han, Z. Zhang, W. Liu, F. Ma, H. Guo, Z. Jiang, X. Wan, A. Wang, C. Yuan, W. Zhou *et al.*, “Theoretical insights into the two-dimensional gallium oxide monolayer for adsorption and gas sensing of C_4F_7N decomposition products,” *Journal of Materials Chemistry C*, vol. 11, no. 35, pp. 11 928–11 935, 2023. [Online]. Available: <https://doi.org/10.1039/d3tc02437g>
- [56] Y. Wang, B. Wang, R. Huang, B. Gao, F. Kong, and Q. Zhang, “First-principles study of transition-metal atoms adsorption on MoS_2 monolayer,” *Physica E: Low-dimensional Systems and Nanostructures*, vol. 63, pp. 276–282, 2014. [Online]. Available: <https://doi.org/10.1016/j.physe.2014.06.017>
- [57] O. D. Agboola and N. U. Benson, “Physisorption and chemisorption mechanisms influencing micro (nano) plastics-organic chemical contaminants interactions: a review,” *Frontiers in Environmental Science*, vol. 9, p. 678574, 2021. [Online]. Available: <https://doi.org/10.3389/fenvs.2021.678574>
- [58] R. F. Bader, “Atoms in Molecules,” *Accounts of Chemical Research*, vol. 18, no. 1, pp. 9–15, 1985. [Online]. Available: <https://pubs.acs.org/doi/pdf/10.1021/ar00109a003>
- [59] R. Ahrling, J. Boy, M. Handwerg, O. Chiatti, R. Mitdank, G. Wagner, Z. Galazka, and S. F. Fischer, “Transport properties and finite size effects in β - Ga_2O_3 thin films,” *Scientific Reports*, vol. 9, no. 1, p. 13149, 2019. [Online]. Available: <https://doi.org/10.1038/s41598-019-49238-2>
- [60] A. Kyrtos, M. Matsubara, and E. Bellotti, “On the feasibility of p-type Ga_2O_3 ,” *Applied Physics Letters*, vol. 112, no. 3, p. 032108, 01 2018. [Online]. Available: <https://doi.org/10.1063/1.5009423>
- [61] A. Zachinskis, J. Grechenkov, E. Butanovs, A. Platonenko, S. Piskunov, A. I. Popov, J. Purans, and D. Bocharov, “Ir impurities in α - and β - Ga_2O_3 and their detrimental effect on p-type conductivity,” *Scientific reports*, vol. 13, no. 1, p. 8522, 2023. [Online]. Available: <https://doi.org/10.1038/s41598-023-35112-9>
- [62] A. J. Green, J. Speck, G. Xing, P. Moens, F. Allerstam, K. Gumaelius, T. Neyer, A. Arias-Purdue, V. Mehrotra, A. Kuramata, K. Sasaki, S. Watanabe, K. Koshi, J. Blevins, O. Bierwagen, S. Krishnamoorthy, K. Leedy, A. R. Arehart, A. T. Neal, S. Mou, S. A. Ringel, A. Kumar, A. Sharma, K. Ghosh, U. Singiseti, W. Li, K. Chabak, K. Liddy, A. Islam, S. Rajan, S. Graham, S. Choi, Z. Cheng, and M. Higashiwaki, “ β -Gallium Oxide Power Electronics,” *APL Materials*, vol. 10, no. 2, p. 029201, 02 2022. [Online]. Available: <https://doi.org/10.1063/5.0060327>
- [63] Y. Yuan, W. Hao, W. Mu, Z. Wang, X. Chen, Q. Liu, G. Xu, C. Wang, H. Zhou, Y. Zou, X. Zhao, Z. Jia, J. Ye, J. Zhang, S. Long, X. Tao, R. Zhang, and Y. Hao, “Toward emerging Gallium Oxide Semiconductors: A Roadmap,” *Fundamental Research*, vol. 1, no. 6, pp. 697–716, 2021. [Online]. Available: <https://www.sciencedirect.com/science/article/pii/S2667325821002144>
- [64] D. Chen, Q. Miao, H. Liao, S. Xiao, B. Xiao, and X. Zhang, “Transition metal (Rh, Pd, and Pt) Doped SnS_2 Monolayer as Promising Work Function Gas Sensors for H_2Se Detection: A

- DFT Study,” *IEEE Sensors Journal*, vol. 24, no. 24, pp. 40 367–40 375, 2024. [Online]. Available: <https://doi.org/10.1109/JSEN.2024.3486563>
- [65] Occupational Safety and Health Administration, “Permissible Exposure Limits - Annotated Table Z-1,” 2026, accessed June 18, 2026. [Online]. Available: <https://www.osha.gov/annotated-pels/table-z-1>
- [66] National Institute for Occupational Safety and Health, “NIOSH Pocket Guide to Chemical Hazards: Nitric Oxide,” <https://www.cdc.gov/niosh/npg/npgd0448.html>, 2026, accessed: 2026-06-23.
- [67] J. H. Davies, *The Physics of Low-Dimensional Semiconductors: An Introduction*. Cambridge University Press, 1998. [Online]. Available: <https://doi.org/10.1017/CBO9780511819070>
- [68] F. Capasso, K. Mohammed, and A. Cho, “Resonant tunneling through double barriers, perpendicular quantum transport phenomena in superlattices, and their device applications,” *IEEE Journal of Quantum Electronics*, vol. 22, no. 9, pp. 1853–1869, 1986. [Online]. Available: <https://doi.org/10.1109/JQE.1986.1073171>
- [69] A. Sibille, J. F. Palmier, H. Wang, and J. C. Esnault, “Observation of Esaki-Tsu negative differential velocity in GaAs/AlAs superlattices,” *Physical Review Letters*, vol. 64, no. 1, pp. 52–55, 1990. [Online]. Available: <https://doi.org/10.1103/PhysRevLett.64.52>
- [70] L. Esaki and R. Tsu, “Superlattice and negative differential conductivity in semiconductors,” *IBM Journal of Research and Development*, vol. 14, no. 1, pp. 61–65, 1970. [Online]. Available: <https://doi.org/10.1147/rd.141.0061>